View metadata, citation and similar papers at core.ac.uk

brought to you by CORE

provided by Edinburgh Research Explorer

THE UNIVERSITY of EDINBURGH

Edinburgh Research Explorer

Application of an intensified narrow channel reactor to the aqueous phase precipitation of barium sulphate

Citation for published version:
McCarthy, ED, Dunk, WAE & Boodhoo, KVK 2007, 'Application of an intensified narrow channel reactor to the aqueous phase precipitation of barium sulphate', *Journal of Colloid and Interface Science* , vol. 305, no. 1, pp. 72-87. https://doi.org/10.1016/j.jcis.2006.08.056

Digital Object Identifier (DOI):
10.1016/j.jcis.2006.08.056

Link:
Link to publication record in Edinburgh Research Explorer

Document Version:
Peer reviewed version

Published In:
Journal of Colloid and Interface Science

General rights
Copyright for the publications made accessible via the Edinburgh Research Explorer is retained by the author(s) and / or other copyright owners and it is a condition of accessing these publications that users recognise and abide by the legal requirements associated with these rights.

Take down policy
The University of Edinburgh has made every reasonable effort to ensure that Edinburgh Research Explorer content complies with UK legislation. If you believe that the public display of this file breaches copyright please contact openaccess@ed.ac.uk providing details, and we will remove access to the work immediately and investigate your claim.

Download date: 11. May. 2020

Application of an Intensified Narrow Channel Reactor to the Aqueous Phase Precipitation of Barium Sulphate

E.D. M^{c}Carthy, W.A.E Dunk, K.V.K. Boodhoo*

School of Chemical Engineering & Advanced Materials, University of Newcastle,

Newcastle upon Tyne, NE1 7RU, UK

* Corresponding author: Email: k.v.k.boodhoo@ncl.ac.uk

ABSTRACT

A homogeneous liquid phase reaction between barium chloride ($BaCl_2$) and sodium sulphate (Na_2SO_4) was conducted in a narrow channel reactor to produce barium sulphate ($BaSO_4$) precipitate. The effects of channel dimensions and channel residence times on crystal size, crystal size distribution, nucleation rates, crystal morphology and conversion of reactants were investigated at different levels of reactant supersaturation ratio.
Our results indicate that the smallest particle sizes are favoured when supersaturation ratios and channel velocities are high. The minimum average particle diameter observed was approximately 0.2 μm in a channel of hydraulic diameter 0.5 mm and length 20 cm at an initial supersaturation ratio of 4483, (0.1M), which correspond to conditions giving rise to the highest nucleation rates. It has also been observed that particle size depends on the conversion to product, the smallest particles being formed when conversion lies within the range 30 to 40%. Conversions in excess of 60% have been reached but there is a detectable limiting effect with increased supersaturation and reduced residence times. Experiments conducted at similar levels of supersaturation under stirred tank conditions showed that particle size was consistently larger and particle size distribution was much broader than that achieved in the narrow channel reactor.
Scanning Electron Microscopy (SEM) images of the crystals formed in the narrow channels show that spherical particles dominate in the smallest channels at high velocities whilst coarse, tabular crystals are obtained in the larger channels. Greater tendency to agglomerate is also observed at high supersaturation ratios, after one minute of reaction.

Keywords: process intensification, narrow channel reactor, barium sulphate precipitation, supersaturation, particle size, particle size distribution, morphology

1.0 Introduction

Intensification is the miniaturisation of process equipment for given duties, while retaining or improving performance. Such a reduction in scale lowers mass and heat transfer resistances allowing reactions to proceed at their inherent rates. Intensified systems are designed at laboratory scale, and scaled out rather than up to achieve the required industrial duty without sacrifice of processing performance.

Narrow channel reactors are among many pioneering technologies at the forefront of the drive towards intensification. They are typified by channel hydraulic diameters of under a millimetre, and may be machined in a variety of substrates from metal to plastic. In addition, the increased surface area -to-volume ratios inherent in reduced geometrical volumes, afford greater heat and mass transfer area, hence reducing temperature and concentration gradients. Such conditions provide the potential for near isothermal, homogeneous conditions to be realistically achieved within the reactor space.

A number of micro-channel reactor studies have been undertaken in the Process Intensification Laboratories at Newcastle University involving organic and aqueous reaction systems [1-3]. These mainly concerned the feasibility of chemical reactions in narrow channels as well as studies of associated flow and mass transport phenomena in immiscible liquid systems.

The present work concerns the precipitation of barium sulphate in narrow channel reactors. Precipitated Barium Sulphate (PBS) is an important industrial product finding many applications in areas including paper-making and the production of paints and pigments. Many of these processes require PBS of a high quality. An industrial-grade barium sulphate product is characterised as one with low mean particle size and narrow particle size distribution, imparting excellent transparency to its substrates, with good water, chemical and light resistances. Abrasiveness is also minimised, a characteristic important to the manufacture of fine coatings.

The accepted standard for the ultra-fine $BaSO_4$ coating grade is approximate to 99.5% below a threshold of 20μm, [4] whereas particles of size less than 100 nm or 0.1 μm are considered *nano*-particles. The high specific surface area of the latter products (> 25 m^2/g) make them ideally suitable for applications in the field of polymer reinforcement, as in the manufacture of composites, bone cement and the control of physical properties such as rheology and viscosity in adhesives and other chemicals. In recent years, there has been a major drive towards the use of these nano-powders in place of the more conventional ultra-fine grades of commercial polymer fillers currently in industrial use. Examples of such nano-composite systems include polypropylene/$CaCO_3$ [5] and poly(methyl methacrylate)/silica [6].

The growing importance of these nanoparticles has inspired the study of precipitation processes in intensified equipment capable of promoting rapid mixing and producing sub-micron or nanoscale particles. Such work has included the use of a Spinning Disc Reactor, where $BaSO_4$ crystals of 0.7 μm in size were produced [7]. A Spinning Cone device was employed in a similar manner in a separate study [8] where mean $BaSO_4$ particle size in the range 0.18 – 0.29 μm was achieved in contrast to a value of 0.75 μm obtained in batch for the same initial supersaturation of 5000. Barium sulphate precipitation in T-mixers has been studied by Nielsen [9-12], Mohanty *et al*. [13], and more recently by Schwarzer & Peuckert [14, 15] where particle sizes in the range 35 – 60 nm have been obtained.

Another recent investigation has involved the application of a narrow channel reactor to a liquid phase calcium carbonate precipitation [16]. Results indicated that rhombic crystals of volume-weighted mean diameter 3 μm and of a narrow size distribution could be achieved under selected operating conditions. The present study seeks to build on this earlier work and further establish the potential of narrow channel technologies in supporting precipitation reactions, particularly that of barium sulphate. An experimental programme has been designed and executed to this effect with results as discussed below. It is hoped that this work will further advance the cause of process intensification solutions to such reactions.

2.0 Materials and Methods

The aim of the experimental work was to characterise the performance of narrow channel devices in precipitating barium sulphate from an aqueous reaction system. The quality and concentration of the precipitate produced are of particular interest in optimising the operation of such channels. The effects of channel dimensions, channel liquid velocity and solution supersaturation on crystal size and size distribution have therefore been examined. We have also carried out batch precipitations of barium sulphate under similar conditions of initial solution supersaturation as benchmarks for the narrow channel precipitation process.

2.1 Design and Fabrication of the Narrow Channel Reactors

Four narrow channels were used in this work each of equivalent length, 20 cm, two of which were straight and contained in one rectangular Perspex© reactor chip (Reactor I), two of which were cut in a serpentine fashion with two 180 degree U-bends, contained in a second separate chip (Reactor II). Schematic diagrams of both reactors are provided in Figures 1 and 2. Each reactor was fabricated by the diffusion bonding of two half plates of Perspex etched with half-channels as illustrated in Figure 3. The cross section of a half channel approximates quite well to an inverted isosceles triangle, each side sloping at equal angles to the surface of the Perspex sheet and at right angles to each other as shown in Figure 3.

The aqueous reactants were introduced into the main reaction channel through a V-mixer which has provision for three feed channels as shown in (Figure 1). However, since only two of the feed channels were required in the current experiments, the third channel was sealed off. The cross-section of each of the feed channels was equal in shape and area to that of the main channel. The feed channels merged into the main reactor channel at point P, (Figure 1, inset). Stainless steel tubing (1.58 mm internal diameter, 75 mm long) was used to direct the reactants into the feed channels from the source syringes. The end of the tubing was connected through a union fitting to a 20 mm long syringe needle. Syringes were manually detachable from the reactor to allow re-charging and flushing.

2.2 Experimental Procedure

A. Preparation Of Solutions

Barium sulphate is produced from aqueous solution by reactive precipitation. The latter process occurs because barium sulphate is effectively insoluble in water and so precipitates out almost immediately upon formation. The solution in this circumstance is said to be supersaturated in $BaSO_4$ because it is present at a concentration in excess of its solubility limit at the solution temperature. Thus in order to effect this reaction, the constituent salt solutions of sodium sulphate and barium chloride, which are both soluble in water, are each prepared to respective concentrations which result in the desired degree of initial supersaturation when the solutions are first contacted. In this way, supersaturation is the driving force of the reactive precipitation or crystallisation, determining the speed of the process and the size and quality of the crystals produced. Because of this effect of supersaturation on the reaction, its influence must always be quantified and distinguished from the separate effects of the reactor environment and operating conditions. This is why the precipitation of barium sulphate in this study was conducted over a range of known initial supersaturation, in order to allow the distinct effects of channel diameter and fluid velocity on the system to be determined.

For each reaction, two 100 ml aqueous solutions of sodium sulphate and barium chloride reagents, (Aldrich), were prepared to the required supersaturation from laboratory stocks. The mass concentrations used were calculated by rearranging equation (1) [17] which expresses the supersaturation ratio of a precipitation system with equimolar stoichiometry. All calculations employ the activities of the ionic species, a_i , in place of their concentrations to reflect non-ideal solution behaviour at concentrations higher than 0.001M [18].

$$S_{act} = \left[\frac{a_A a_B}{K_{sp}} \right]^{1/2} = \left[\frac{\gamma_A c_A \gamma_B c_B}{K_{sp}} \right]^{1/2} \quad \textbf{(1)}$$

Here $a_a = a_b$ on a stoichiometric basis and $\gamma_A = \gamma_B = \gamma$ as both the Ba^{2+} and SO_4^{2-} ions possess valence of equal magnitude, ($|z_A| = |z_B| = 2$). Using equation (2), the common Debye-Huckel (DH) activity co-efficient is

calculated from a knowledge of the ionic strength, I, of the solution given by equation (3) [19]. The DH activity coefficient is used to model long range interactions between charged species.

$$\gamma = exp\left[\frac{-0.51z^2\sqrt{I}}{1+\sqrt{I}}\right] \quad \textbf{(2)}$$

$$I = 0.5\sum c_i z_i^{\,2} \quad \textbf{(3)}$$

The re-arranged form of equation (1) in terms of the initial mass concentrations, m_i, of the respective salts is:

$$m_i = M_i\sqrt{S_{act}^{\,2}K_{sp}}\Big/\gamma \quad \textbf{(4)}$$

With a solubility product, K_{sp}, of 1.1 x 10^{-10} mol^2 dm^{-6} for the barium sulphate system at 298K [18] the initial concentrations of $BaCl_2$ and Na_2SO_4 may be calculated on a mass basis for a desired value of S_{act}, using equation (4) and a knowledge of the respective molecular weights, M_i, of barium chloride and sodium sulphate.

B1. Reaction Procedure in Narrow Channels

Two 10 ml syringes were charged with sodium sulphate and barium chloride reactant solutions to their full 10 ml capacity respectively. The syringes were seated in two parallel slots, and the syringe push plate was positioned so as to achieve simultaneous initial contact with the heads of each syringe. The speed of the syringe driver mechanism was adjusted to deliver the required channel velocity according to Table 3 and the power was switched on. The syringes discharged into the narrow channel, and the resulting solution was collected at the outlet tube. The driver was switched off once the syringes had completely expelled all of their contents. Two other syringes were charged with distilled water and used to flush the reactor channel as soon as possible to discharge any scale which may have become lodged there. This was important for two reasons: to avoid fouling and channel blockage, and to prevent the analysis of solution concentration and PSD being distorted by older material during subsequent runs.

B2. Reaction Procedure in Stirred Tank Reactor

0.1 M solutions, (S_{act} = 4483), of sodium sulphate and barium chloride were prepared consistent with the procedure in Section A. 500 ml of the former solution was transferred to a beaker having a capacity of 1 litre, and an impeller was activated to a speed of approximately 250 rpm to provide a sufficiently well-mixed environment. 500 ml of the second solution was poured in, allowing the precipitation reaction to proceed. A homogeneous, milky dispersion was formed throughout the beaker within one second, indicating that the chosen agitator speed was adequate to effect reaction throughout the bulk. Between 1.5 – 3.0 ml of precipitate sample was drawn off by pipette after 5 seconds reaction, diluted in 100 ml distilled water and immediately submitted for laser diffraction analysis. Sample volume was varied in each individual case to achieve the necessary laser obscuration for a meaningful measurement as described in more detail in the next section.

C. Analysis of Samples

The samples were analysed offline, within 30-60 s of collection from the reactor, in a Malvern Mastersizer 2000 unit for the determination of mean crystal size and crystal size distribution. Rapid analysis of the samples was essential to prevent considerable agglomeration of the crystals which typically set in 60 seconds after collection. Such an effect was consistently observed for five selected samples across the experimental range by studying the evolution of the crystal size distribution in real time between 30 and 120 s after collection. Typically, the Sauter mean diameter, d_{32}, of these samples rose from a value in the range 1 – 10 μm measured at 30 s after collection to a stable terminal value in the range 15-22 μm at 120 s after collection.

A typical diffraction measurement was executed in the following manner:1 - 3 ml of the newly-formed suspension were diluted in a continuous circulation of 100 ml de-ionized water within the Mastersizer. As stated previously, the extent of dilution in each individual case was determined by the requirement to achieve an optimum 12% obscuration of the diffraction laser beam, and varied with initial supersaturation according to Table 4. This was because the opacity of the suspension increased with supersaturation; thus lower sample volumes were required to achieve the desired laser obscuration at higher initial supersaturations. Samples were added drop-wise to the

circulation, where necessary, to ensure a minimum of error in subsequent calculations for precipitate yield. The volume fraction of precipitate present was returned by the accompanying software in units of parts-per-million. The latter was multiplied by the dilution factor to obtain the precipitate yield of the sample, from which conversion was calculated. Comparison of these results with specimen gravimetric analysis returned an error of ± 5%. Thus conversion data are indicative only.

The particle nucleation rate was calculated as the ratio of the particle count detected to the precipitation induction time. The latter was inferred from the length of clear liquid persisting between the mixing point P in Figure 1, (inset), and the onset of opacity in the channel. This method was first used by Nielsen [10] for $BaSO_4$ precipitation in a T-mixer. The transparent induction segment determined for the narrow channel was typically between 1 and 2 mm long. The ratio of this segment to the entire channel length was multiplied by the channel residence time to derive an estimate for induction time. This approach was justified by a minimum of fluctuation, (2 – 3%), in the mean axial fluid velocity in the channel. Induction time inferred by the above method was found to vary in the range 1 – 32 ms, corresponding to minimum and maximum channel residence times of 0.9 and 6.5 s respectively. Calculated alternatives to the observed induction times are discussed in Section 3.4

To study the morphology of the barium sulphate crystals, Scanning Electron Microscope, (SEM) analysis was conducted on filtered, dried samples of barium sulphate precipitate, (Machine model: JEOL 5300 Low Vacuum).

3.0 Results and Discussion

The findings relating to the individual effects of channel diameter, mean axial channel fluid velocity and initial solution supersaturation on Sauter diameter, particle nucleation rate and precipitate conversion are presented below. The Sauter diameter, or surface-weighted mean diameter, d_{32} is defined as the ratio ($\Sigma N_i d_{pi}^3 / \Sigma N_i d_{pi}^2$) [20] where N_i and d_{pi} are the particle count and size respectively measured in each size category i of the diffraction measurement spectrum.

It is worth noting that, because of the inevitable time delay of 30-60 s incurred in obtaining offline CSD measurements by laser diffraction, the particle sizes reported in the following sections may be slightly higher than the actual particle sizes in the sample collected at the reactor outlet. Although high residual supersaturation is expected to contribute to significant crystal growth after collection of an undiluted sample from the outlet of the channel reactor, our dilution and rapid analysis procedures ensure that this effect is minimised so that the measured particle sizes and their distributions are representative of the suspension quality at the outlet of the channel, even if they may be somewhat conservative. In order to quantify this assertion, we have compared our experimental measurements of particle size with values predicted by an established crystal growth model. The model, formulated by Mersmann [21],[22] is applicable to diffusion-limited crystal growth and is expressed simply as a function of the prevailing mass transfer co-efficient and the residual supersaturation of the solution (equation (5)). The application of the model is subject to the criterion in (6) being fulfilled.

$$G_{diff} = k_m \frac{\Delta c}{c_c} = k_m \left(\frac{c_{res} - c^*}{c_c} \right) \quad \textbf{(5)}$$

$$\left(S_{res} - 1\right) > 0.01 \sqrt{\frac{c_c}{c^*}} \quad \textbf{(6)}$$

As an example to illustrate our comparison, we have applied the growth model to predict the crystal size in the precipitating mixture in the main channel segment and in the subsequent diluted analyte suspension collected from the channel exit and analysed in the laser diffraction unit. The effect of residual supersaturation on crystal growth will be most significant at the highest initial supersaturations and lowest conversions achieved in the channel. We have therefore based the crystal growth estimation on the following set of conditions: $S_{act,0}$ = 4483, (c_0 = 0.105 M), d_h = 0.5 mm, Re = 1025, X = 15%. The corresponding residual ion concentration in the solution, c_{res}, is 0.089M giving a corresponding residual supersaturation, S_{res}, of 3968 with an activity coefficient of 0.46 using equations (1) to (3). With a solubility, c*, of 10^{-5}M, molar crystal density c_c of 19.3M for barium sulphate and a diffusion limited mass transfer coefficient of the order of 10^{-4} m s^{-1}, a crystal growth rate of 4.6 x 10^{-7} m s^{-1} is obtained in the channel. If this growth rate is applied representatively over the 0.2 m length of the main channel

segment, (with residence time of approximately 0.1 s), a value of d_{32} = 0.05 μm is anticipated at the channel outlet. If 1.5 ml of the product sample is then diluted in 100 ml of flowing distilled water in the laser diffraction unit, a lower residual ion concentration of 1.32 x 10^{-3} M.and residual supersaturation of 110 are obtained in the analyte suspension flowing within the *Malvern* instrument. The resulting growth rate is 6.8 x 10^{-9} m s^{-1}, two orders of magnitude lower than that obtained for the original product suspension in the narrow channel. Thus, a mean crystal size of 0.2-0.4 μm is predicted after an analysis period of 30-60 s in the laser diffraction unit, representing the largest crystals which can be expected solely as a result of the effect of residual supersaturation in the diluted analytes. As will be seen in the following sections, mean crystal sizes in the range 0.2-10 μm were achieved experimentally under a range of operating conditions. Whilst the residual supersaturation effects on crystal growth in the diffraction unit may be said to contribute significantly to the crystal size in the lower size range (<1 μm), this is however limited to only a small proportion of crystals produced in the narrow channels. In fact, this highlights that the smallest crystal sizes presented in this work is conservative and it would be reasonable to expect that actual particles at the channel exit may indeed be much smaller than the measurements obtained. Nevertheless, it should be borne in mind that the data should be rather treated as indicative of the relative effect of reactor conditions on particle quality and precipitate yield than as absolutely representative to a high accuracy.

3.1 Particle Sauter Diameter

Increased supersaturation, higher mean axial channel velocity and reduced channel diameter are favourable conditions in the production of ultra-fine particles as evidenced in Figures 4 (a) and (b).
Particle mean size decreases with lower channel hydraulic diameter and higher supersaturation (Figure 4(a)), and with higher channel Reynolds Number, Re = (Vd_h/ν) (Figure 4(b)). The observed effect of increased supersaturation is well established in the crystallisation literature and is to be expected. However, the influence of channel diameter and fluid velocity are particular characteristics of this narrow channel system. We believe that such effects on particle size are due to the influence of reactor conditions on mixing and nucleation rates.

A significant instance of particle diameters below 1 μm is evident for the channel reaction, especially at velocities in the region of V = 2.0 ms^{-1} at S = 4483, d_h =0.5 mm, where the finest particles are precipitated, Figure 4(a). This equates to Re = 1025, a value which is relatively low when compared with some other systems in the literature, [14]. The hydrodynamic effects of the narrow channel are easily reproducible and are controlled by means of adjusting reaction parameters such as liquid flowrate and channel diameter. This provides a greater degree of flexibility in "tuning" precipitation conditions than appears possible for the stirred batch reaction. More importantly, there are strong indications of a potential to produce particles approaching nano-size range, within narrow channels, at supersaturation ratios in excess of 1758. The application of appropriate surfactants to reacting solutions and internal surface coatings to channels may well provide the means to achieve further reductions in mean particle size.

3.2 Particle Size Distributions

Figure 5(a) illustrates the significant difference in particle size distribution between barium sulphate precipitated in the 1 litre stirred batch reactor and that generated in a 0.5 mm diameter channel at a common supersaturation level of 4483. The channel PSD is obtained for a channel residence time of 0.1 s. The reproducibility of the 0.5 mm PSDs is demonstrated by Figure 5(b). It is clearly observed that the "agglomeration tail" characteristic of the stirred tank reaction is considerably reduced in the narrow channel. This could be due to a number of factors. Firstly, the residence time in the channel is an order of magnitude smaller than that incurred in the batch reaction i.e. 0.1 s compared with 5 s. Thus it is likely that there is insufficient time for significant crystal growth and agglomeration to occur within the channel and during the subsequent analysis period of less than 60 s. Secondly, the size of primary particles produced may be smaller because the hydrodynamic conditions in the channel favour particle nucleation over crystal growth, the two primary processes which compete for residual supersaturation in a crystallising solution.

3.3 Micromixing and Nucleation Rate

Figures 6 and 7 provide a graphical summary of particle nucleation rate in the narrow channels. Nucleation rate is intimately associated with the degree of micro-mixing present in a precipitation system [14]. Higher nucleation rates normally indicate a better quality of micro-mixing.

Nucleation rates demonstrate sensitivity to supersaturation, velocity, and channel internal diameter. High supersaturations favour higher nucleation rates, and there is also a significant rise in nucleation rates from 10^{14} to 10^{21} nuclei m^{-3} s^{-1} as channel velocity is increased over the experimental range $0.05 < V < 2.0$ ms^{-1}. This corresponds to Re in the range $62 < Re < 1025$.

There is also evidence that the use of narrower channels increases the nucleation rate over a similar range of approximately six orders of magnitude. Precipitations in Channel B (d_h=1.5 mm) are characterised by rates of nucleation four magnitudes higher than those performed in Channel A (d_h=2.0 mm), while precipitations occurring in Channel S2 (d_h=0.5 mm) appear to exhibit the highest nucleation rates (five orders of magnitude higher than those observed in Channel A). We believe that these results indicate better mixing in narrower channels. Such an argument has already been advanced by Trippa *et al.* [16] where $CaCO_3$ was precipitated in channels of similar size and cross-section. In that work, a determination of specific power input per channel, ε, was employed as an index of mixing intensity after [23]. In a similar treatment of channel mixing in this work, two parameters are used: the specific power input to the channel, ε, according to [16] and the Peclet number, Pe. A high value of the former is taken to indicate good micro-mixing performance, while the latter is an established parameter [24] which presents a quantitative relationship between convective and diffusive mass transport in a continuous flow system. The specific power input to a given channel is calculated from a knowledge of the total power supplied to the system, P, calculated as the product of channel pressure drop, ΔP, and fluid volumetric flowrate, Q, according to equation (7) [16]:

$$P = Q.\Delta P = Q.\frac{2\rho V^2 fL}{d_h} \qquad \textbf{(7)}$$

Here L represents the channel length, including channel lead and tail tubing, and both reactant channels in the V-mixer. P is the fluid density and d_h is the channel hydraulic diameter. f is the channel friction factor which is assumed to be 14.2 / Re for laminar flow in square channels [25]. Specific power input, ε, is calculated as the ratio of total power supplied to the mass of fluid in the narrow channel reactor at any instant according to equation (8) from [16]

$$\varepsilon = \frac{\boldsymbol{P}}{\boldsymbol{Q}\rho\tau_{res}} = \boldsymbol{28.4}\nu\frac{\boldsymbol{Q^2}}{\boldsymbol{d_h^6}} \qquad \textbf{(8)}$$

From equation (8), it is observed that specific power input, hence mixing intensity, increases significantly with rising fluid flowrate Q, but a much larger increase is caused by the reduction of channel diameter d_h. Figure 8 illustrates these effects more clearly for the range of conditions used in this study.

The specific power input is seen to rise significantly with Re as expected, but it is increased by orders of magnitude when the channel diameter is reduced. Increased power input translates into greater mixing intensity. This provides further quantitative evidence for the contention that the narrowest channels provide the best mixing conditions as already attested by the high nucleation rates observed for the 0.5 mm channel, (Figure 6(a)). However, it must also be realised that such an improved mixing performance incurs significantly higher pressure drop, (Figure 8(b)), with implications for effective fluid delivery.

3.4 Induction and Mixing Times In The Y-Junction

As stated earlier, the particle nucleation rate was calculated as the ratio of the particle count detected to the precipitation induction time. Incorporated within the induction time is the effective mixing time, the magnitude of which may have an effect on the real induction time of the system and the nucleation rate. The term *effective* is used to distinguish the macro-mixing mechanism in the induction segment from that in the main channel segment, which is necessarily inhibited, especially in the radial direction, because of diffusion-limitation in the laminar flow regime as discussed in Section 3.5.We present in this section an analysis of the mixing in an attempt to estimate the mixing time in our narrow channels.

Roelands *et al.* [26] estimated the total available mixing time, $t_{mix,i}$, in a Y-junction using equation (9):

$$t_{mix,i} \approx t_{ind} = \frac{L_{ind}}{V} \qquad \textbf{(9)}$$

On the basis of equation (9) and a maximum transparent induction segment L_{ind} of 1 mm as a conservative estimate in this work, the range of available mixing (or induction) time applicable to our study is $0.5 < t_{mix,,\,i} < 32$ ms (for $0.5 < d_h < 2.0$ mm). A theoretical expression for the induction time of crystallisation, as applied to barium sulphate precipitation, is provided by Carosso and Pelizzetti [27] in terms of temperature and supersaturation (equation (10)). The model does not employ any hydrodynamic terms, depending solely on properties of the crystallising species.

$$t_{ind} = \exp\left[\frac{B}{T^3(\log S)^2} - A\right] \qquad \textbf{(10)}$$

With experimentally determined values of 4.2 and 15.51 for A and (B/T^3) applicable to barium sulphate precipitation [26], equation (10) theoretically predicts induction times of $48 < t_{ind} < 101$ ms in the present work for $707 < S_{act} < 4483$. However, at the maximum channel residence time of 6.5 s and maximum supersaturation, the experimentally determined highest induction time is approximately 32 ms. These data clearly demonstrate that hydraulic conditions within the channel Y-mixer play an important role in significantly reducing the induction time of crystallisation.

Two principal mixing regimes are possible within the Y-mixing junction: the disintegration of turbulent fluid eddies according to the description of Baldyga and Bourne [28] and a laminar mixing regime put forward by Villermaux [28] where fluid layers are stretched and folded. Both models will be considered in the present context.

Considering the possibility of turbulent mixing activity within this induction segment as stipulated by Baldyga and Bourne [28], a progressive size decay of large eddies in a Y-junction to sizes at the molecular level occurs. This is represented by a succession of decreasing mixing length and time scales i.e. inertial-convection mixing, (τ_S), to micro-mixing at the Kolmogorov scale, (τ_E), to molecular diffusion at the Batchelor scale, (τ_{diff}). The expressions for these mixing times and their characteristic length scales are reproduced in Table 5 (equations (11) – (16)). It is clear that dramatic reductions in mixing time can be effected at every mixing scale by increasing the specific turbulent energy dissipation rate, ε_{turb}. From equation (11), it is evident that both increasing velocity and decreasing channel hydraulic diameter are the means of achieving this. Moreover, since $\varepsilon_{turb} \alpha V^3$, increase in mean velocity is the more effective strategy. The present work provides a velocity range $0.03 < V < 2.05$ ms^{-1} which results in a closely controllable ε_{turb} range of 0.001 – 482 W kg^{-1}. When it is considered that Sauter mean

diameter is reduced from 10.7 to 0.2 μm over this range of channel velocities, the argument in favour of a Y-junction micro-mixing mechanism under turbulent conditions is compelling.

Villermaux [29] presented an alternative analysis of mixing for a laminar flow regime in a narrow channel. The mixing process was presented as a striation or "stretching" and folding of fluid layers in the presence of a convective velocity field, a phenomenon recognized to generate micromixing below the Kolmogorov length scale [30]. A correlation for laminar micro-mixing time based on modifications of the Baldyga & Bourne expression for turbulent micro-mixing time was produced (equation (17)):

$$t_{mic} = \sqrt{\frac{2\upsilon}{\varepsilon}} \qquad \textbf{(17)}$$

where ε is defined as in equation (8) for laminar flow

Thus, from equation (17), for the slowest flow condition (Re = 62, ε = 0.072 W kg^{-1}), the micro-mixing time is t_{mic} = 17 ms, whereas for the fastest flow generated in the 0.5 mm channel (Re = 1025, ε = 115 W kg^{-1}), a value of 0.1 ms is obtained.

A comparison of corresponding induction and micro-mixing times calculated by equations (10) and (17) respectively for the lowest supersaturation of S_{act} = 707 shows that at Re = 62, t_{mic} = 17 ms which is approximately 35% of the minimum theoretical induction time of 48 ms, (and 53% of the estimated experimental value of 32 ms), whereas at Re = 1025, t_{mic} = 0.1 ms which is two orders of magnitude lower. Thus, according to Villermaux's equation (17), micro-mixing time is consistently less than the theoretical induction time for the entire range of conditions in the present work.

This is not so if a turbulent micro-mixing mechanism is posited. Here, a maximum bound [Re = 62, t_{mic} = 545 ms] is indicated, which is an order of magnitude higher than the observed value of t_{ind} = 32 ms. Insufficient time is afforded by even the maximum observed induction period (32 ms) for effective micro-mixing to take place, causing precipitation at this value of Re to be limited by micro-mixing. However, increasing Re to 1025 results in a dramatic reduction of t_{mic} to 0.78 ms, providing excellent micro-mixing which is two orders of magnitude faster than the overall induction process. Defining a critical Re for which (t_{mic} / t_{ind}) = 1 and below which micromixing begins to limit precipitation, critical Re values of 23 and 40 may be calculated in the 0.5 mm diameter channel at S_{act}= 707 and 4483 respectively. As a maximum Re of 1025 was achieved experimentally in that channel, it was not only relatively easy to operate above these thresholds, but also to reduce the ratio (t_{mic} / t_{ind}) to 0.016 at S_{act} = 4483 and maximum throughput, allowing rapid micro-mixing relative to the total induction period.

In addition, because micro-mixing occupies a much smaller fraction of the induction period at higher Re (e.g. (t_{mic} / t_{ind})= 0.016 at S_{act} = 4483 and Re = 1025), there is greater confidence in nucleation rate values calculated from visual induction time. Thus for the turbulent mixing model applied to the 0.5 mm channel, discrepancies between actual and calculated nucleation rates are only significant (> 5%) for Re < 263 at S_{act}= 707 and Re < 453 at S_{act}= 4483. Therefore the minimum pressure drops incurred to maintain these rates of micromixing at either supersaturation are 1086 and 2809 Pa respectively.

In contrast to the 0.5 mm channel, conditions in the channel of d_h = 2 mm are insufficient to effect adequate micro-mixing. Minimum Re values required to maintain the ratio (t_{mic} / t_{ind}) below 0.05 would be 1565 and 2693 at S_{act} = 707 and 4483 respectively. However, the maximum Re generated at full pumping power in the 2 mm channel was 455 which is well outside the range required for efficient mixing. In order to achieve the higher Re values for good mixing, pressure drops of 2319 and 5998 Pa would have been incurred at either supersaturation. When the latter are compared with pressure drops incurred in the 0.5 mm channel to achieve a 5% micro-mixing period (1086 and 2809 respectively), it is seen that the 0.5 mm channel is more effective as a mixer requiring less specific energy input ε at lower pressure drops to promote good mixing.

Under the laminar mixing model according to Villermaux [29], the nucleation rate which is calculated from visual induction time (32 ms) is a conservative estimate which is approximately 53% lower than the true value at Re =

62, since micromixing dominates at least the first 17 ms of the induction period, prior to nucleation and growth. The difference between calculated and actual nucleation rate diminishes to insignificance at Re = 1025, as t_{mic} falls to 0.1 ms. Thus the ability to both achieve and control rapid micro-mixing by manipulating channel Re is indicated.

In summary, if micro-mixing is assumed to occur under laminar conditions, the hydraulic environment provided by the Y-mixer is sufficient to ensure that micro-mixing time is significantly lower than induction time. Operation above critical values of Re ensures similar performance according to the turbulent mixing model. Confidence can therefore be expressed in estimates for nucleation rate based on observed induction time as presented in this study, especially at higher values of Re, for which t_{mic} diminishes in both the laminar and turbulent models.

3.5 Mass Transfer In Main Channel Segment

Two main mechanisms of mass transfer are possible in the main channel segment, namely convective mass transfer in the axial direction and diffusive mass transfer in the radial direction. Axial diffusion is considered to be negligible since longitudinal movement in the channel is dominated by convection. In order to assess the nature and degree of mass transfer taking place in the channel, it is helpful to determine the relative contributions of these two mechanisms to the total mass transfer. One way of doing this is by use of the Peclet Number, Pe. This is defined as the ratio of mass transfer occurring by convection in a system to that occurring by diffusion [24]. It may also be represented as the product of the Reynolds and Schmidt Numbers according to equation (18). It was used by Barresi *et al.* [31] to characterise mixing for a barium sulphate precipitation in a Couette reactor. We have adopted a similar approach in our analysis.

$$Pe = \mathrm{Re}\,Sc = \left(\frac{Vd_h}{\nu}\right)\left(\frac{\nu}{D}\right) = \frac{Vd_h}{D} \qquad \textbf{(18)}$$

The range of Pe applicable in the present work has been $0.5 \times 10^6 < Pe < 1.025 \times 10^6$, values indicating the dominance of convection over diffusion under the flow regime obtaining in the channel. The calculation assumes a limiting diffusion co-efficient of 1.065×10^{-9} m^2 s^{-1} for the ionic species participating in the reaction (SO_4^{2-} and Ba^{2+}) [32].

Effects of Peclet number on Sauter diameter and precipitate conversion respectively are shown in Figure 9. In Figure 9(a), it is clear that reduced particle size coincides with an increase in Peclet Number. As stated earlier, it is again seen that reduced channel diameter results in smaller mean particle size. Thus, in this context, reduced particle size is most directly linked to increased velocity at any given channel diameter.

In contrast, as highlighted in more detail in the next section, precipitate conversion does not benefit from high Pe (Figure 9(b)) and the implied dominance of convective transport in the manner which might be expected. This is probably because channel residence time has been reduced from between 6 s in the larger channels to 0.1 s at the highest flowrate in the 0.5 mm channel.

The expression of Chakroborty [33] (equation 19), may be used to generate an absolute estimate for the radial diffusion time of ions in the channel.

$$t_{diff} = \frac{d_h^2}{D} \qquad \textbf{(19)}$$

Under this definition, the range of diffusion time imposed in the present work is 2.5×10^2 s $< t_{diff} < 4.0 \times 10^3$ s, confirming, as expected, that radial diffusion in the main channel segment is severely limited. This is because the maximum residence time of a fluid element in this experiment was 6.5 seconds.

Convective mass transport may be indirectly quantified by considering the radial shear rate profiles in the main channel segment. Any convective transport which does take place in a channel may be expressed in terms of the laminar shear forces generated. These may be quantified by a radial shear rate profile across the channel and are

calculated by firstly estimating the corresponding radial velocity profile of fully developed laminar flow in the channel using the velocity distribution for laminar flow (equation (20)) based on the Poiseuille equation [34]. Here, u = u_{max} along the axial centre of the channel where r = 0 (and u_{max} = 2V under laminar flow conditions), and u = 0 at the channel walls where r = R.

$$u(r) = \frac{\Delta P}{4\mu L}\left(R^2 - r^2\right) = u_{\max}\left(1 - \frac{r^2}{R^2}\right) \quad \textbf{(20)}$$

The shear rate at any radial position in the channel may be expressed as the velocity gradient along the radial vector of the pipe, equation (21), which is derived from the differentiation of equation (20):

$$\gamma = \left|\frac{d\left(u(r)\right)}{dr}\right| = \left|\frac{-2u_{\max} r}{R^2}\right| = \left|\frac{-4Vr}{R^2}\right| \quad \textbf{(21)}$$

The resulting shear rate profiles for flow conditions tested in the narrow channels in the range 61 < Re < 1025 are reproduced in Figure 10. It is seen that, theoretically, a condition of zero-shear is expected at the centre-line, with shear increasing linearly in the radial direction to varying maxima depending on the value of the Reynolds number and channel diameter. Increased Re and reduced channel diameter, d_h, coincide with increased fluid shear rates, with the lowest wall shear rate of 123 s^{-1} in the largest channel (d_h=2 mm) at Re=62 approaching a maximum of 32800 s^{-1} at the channel wall for Re = 1025, d_h = 0.5 mm. The corresponding incidence of convective mass transfer which is determined by shear rate in the fluid layer therefore increases as the size of the channel is reduced and flowrate increases.

From the preceding micro-mixing time and mass transfer analysis, it is seen that mixing in the induction segment of the channel immediately after introduction of both reactant streams at the Y-junction and convective mass transfer in the main channel both have an impact on the precipitation of barium sulphate in the channel. Overall, the analysis serves to demonstrate that by employing narrower channels and generating high mean fluid velocities, crystallisation mixing times may be reduced and convective mass transfer rates may be increased by orders of magnitude to give reduced mean primary particle size.

3.6 Conversion

Precipitate conversion, as determined by laser diffraction measurement, does not appear to be affected in a definite manner by either channel diameter or Reynolds number. This is indicated by the mutual variance of trends shown in Figure 11 (a). Supersaturation seems to have a more definite effect on conversion. This is evidenced by Figure 11 (b) where a conversion maximum is detectable in the range S = 1700-2200 in channels of different diameters operating under the hydrodynamic conditions indicated. Also, there appears to be a slight correlation between conversion and channel residence time from the data presented in Figure 11(b) whereby, at longer residence times, higher conversions are achieved suggesting that consumption of soluble ions in nucleation and/or crystal growth is encouraged under such conditions. This effect is more apparent in the lower range of supersaturation ratios.

3.7 SEM Analysis and Morphology

Images from the SEM analysis of barium sulphate precipitate are provided in Figures 12 and 13. Particles in Figure 12 appear to be ultra-fine and largely independent with an absence of any comprehensive agglomeration. There is also evidence of spherical particles and some tabular crystallites with low aspect ratios. However at S = 4483 (Figure 13(a)), it can be seen that there is a predominance of spherulites, and evidence of agglomeration is clearly visible. The wider channel, B (d_h=1.5 mm), tends to produce coarser, more tabular particles (Figure 13(b)), which are also severely agglomerated at the same supersaturation ratio. As a result it would seem that supersaturation ratios must be restrained in order to derive any benefit from reduced primary particle sizes, regardless of what production methods or conditions are employed.

4.0 Conclusions

Narrow channel reactors have been shown to support the aqueous precipitation of barium sulphate over a significant range of initial supersaturation, $707 < S_{act} < 4483$ and mean axial velocity $0.5 < V < 2.0$ m/s. Mean crystal sizes as fine as 0.2 μm Sauter mean diameter have been measured in channels of 0.5 mm internal diameter. Such results have been observed at the highest solution supersaturation investigated, $S_{act} = 4483$, consistent with initial reactant concentrations of 0.1 M $BaCl_2$ and Na_2SO_4 respectively. However, conversions in excess of 60% are best achieved at supersaturations below $S_{act} = 2634$, so that optimisation between precipitate quality and mass yield is required.

Micro-mixing in the induction segment of the channels is discussed. Two mechanisms are investigated: the first based on turbulent dispersion of eddies and the second concerning a fluid-layer folding model in laminar flow. In the first model, micro-mixing limits precipitation for flow in a channel below a critical Reynolds number, which is dependent on the value of initial supersaturation. The criterion for this is $(t_{mic} / t_{ind}) > 1$. Conversely, the laminar model predicts that micromixing times are always significantly lower than theoretically predicted induction times over the entire range of conditions tested. Increasing Re reduces the fraction (t_{mic} / t_{ind}) to below 0.01 at Re = 1025, so that estimates of nucleation rate derived from visual induction time are considered reasonably accurate at high Re. Furthermore, convective mass transfer in the main channel segment, estimated by shear rates generated in the fluid layers formed under laminar flow conditions, becomes increasingly important in smaller channels operating at relatively high Re. Overall, it is observed that higher levels of micro-mixing and convective mass transfer achieved in narrower channels operating under conditions of high mean fluid velocities produce particles of smaller Sauter mean diameter.

SEM imaging corroborates the particle size data obtained by laser diffraction, indicating the formation of sub-micron $BaSO_4$ crystals under certain processing conditions. Tabular morphology and larger crystals are observed in wider channels, with smaller, spherical particles being produced in the 0.5 mm channels at high fluid velocities. Qualitative evidence that higher supersaturation ratios encourage severe agglomeration of fine nuclei, some 60 s after reaction, is also presented. Study of the time evolution of specimen CSDs have shown that agglomeration is typically delayed until 60 s after reaction, (30 s after laser diffraction analysis), so that the CSD data presented is representative of the true channel precipitate quality as collected at outlet.

The mass production rate of one of the best performing channels, (I.D. = 0.5 mm), is 2.59 mg s^{-1} .This represents an output of 9.32 g h^{-1}, (0.22 kg / day), with a specific power input of 50 to 100 W kg^{-1} at a channel pressure drop of 0.1 bar. At this rate, with a channel flow of 0.5 ml s^{-1} of precipitating solution, over a tonne of barium sulphate may be produced by 4500 such 0.5 mm channels per day. The potential of such channels to provide a continuous source of ultra-fine particles for a wide range of applications is promising. Such output can be attained by the scale-out of these channels to many thousands operating in parallel, according to a “cassette” model. Appropriate manifolding, precise micro-fluidic delivery and the avoidance of fouling in such systems remain the primary challenges in converting such technology to wide industrial usage. Further research is anticipated to include the addition of in-line surfactants and the surface coating of channels in order to minimise fouling and post-reaction agglomeration. A reduction in primary particle size from the present minimum of 0.2 μm to below 0.1 μm i.e. to nano-scale, in this type of narrow channel system is also envisaged. The means to do this have already been advanced in the two recent studies by Schwarzer *et al*.[14]. Such measures include control of the initial barium-to-sulphate ion ratio: increasing the latter has reduced both primary particle size and aggregation during and immediately after precipitation of the product. The further development of in-situ analysis techniques at the micro-scale should also improve the characterisation of particles and promote a deeper understanding of the crystallisation process in intensified environments.

Acknowledgements

JIF funding of the Responsive Processing Laboratories where this work was undertaken is gratefully acknowledged. We would also like to thank all colleagues who have contributed to this work.

Nomenclature

Symbol	Variable	Unit

c	Concentration of species	mol dm^{-3}
c^*	Solubility of species	mol dm^{-3}
D	Diffusion coefficient	m^2 s^{-1}
d_h	Channel hydraulic diameter	mm or 10^{-3} m
d_{pi}	Particle size in size category i	μm or 10^{-6} m
d_{32}	Mean Sauter diameter	μm or 10^{-6} m
ε	Specific pump energy input	W kg^{-1}
ε_{turb}	Specific turbulent energy dissipation rate	W kg^{-1}
f	Friction factor	-
F	Dilution Factor	-
I	Ionic strength of solution	mol dm^{-3}
K_c	Solubility product	mol^2 dm^{-6}
k_m	Mass transfer coefficient	ms^{-1}
L	Length of narrow channel reactor	m
m_i	Mass concentration of species $_i$	mol dm^{-3}
N_i	Number of particles in size category i	-
ΔP	Pressure drop	Pa or N m^{-2}
Pe	Peclet number = (V d_h /D)	-
Q	Volumetric fluid flowrate	m^3 s^{-1}
R	Radius of narrow channel	mm or 10^{-3} m
r	Channel radial co-ordinate	mm or 10^{-3} m
Re	Reynolds number = (u d_h / ν)	-
S_{act}	Supersaturation ratio (activity basis)	-
S_{res}	Residual supersaturation ratio	-
Sc	Schmidt number = (ν / D)	-
T	Temperature	K
t_{diff}	Time of transverse diffusion in channel	s
t_{ind}	Time of precipitation induction	ms or 10^{-3} s
t_{mic}	Time of micromixing in laminar flow	ms or 10^{-3} s
t_{res}	Residence time in Channel	s
$t_{mix,i}$	Time of total mixing	ms or 10^{-3} s
$u(r)$	Axial velocity at radial position r	m s^{-1}
V	Mean axial channel velocity	m s^{-1}
V_s	Sample volume analysed in diffraction unit	ml or 10^{-6} m^3
z_i	Valence of ionic species i	-
ν	Kinematic viscosity	m^2 s^{-1}
ρ	Fluid density	kg m^{-3}
τ_{diff}	Molecular diffusion time (Batchelor scale) in turbulent mixing	ms or 10^{-3} s
τ_E	Micro-mixing time (Kolgomorov scale) in turbulent mixing	ms or 10^{-3} s
τ_s	Inertial-convection mixing time in turbulent mixing	ms or 10^{-3} s
μ	Fluid viscosity	Pa s
γ	Activity coefficient	-
η_K	Kolmogorov length scale	μm or 10^{-6} m
η_B	Batchelor length scale	μm or 10^{-6} m

Subscripts

c	crystal
res	residual

References

1. J. Burns, C. Ramshaw Trans.IChemE, 77, 1999,206-211.
2. J. Burns, C. Ramshaw in: W. Ehrfeld,(Ed.) Fourth International Conference on Microreactor Technology, Atlanta, U.S.A., 2000,133 - 140.
3. J. Burns, C. Ramshaw, R.S.C. Lab-on-a-Chip Journal, 1 (2001), 10-15.
4. J.P. Searls, Mineral Commodity Survey: Barite, U.S. Geological Survey, 2005.
5. C.M. Chan, J. Li, Y.K. Cheung, Polymer, 43 (2002), 2981-2992.
6. Y.T. Wang, T.C. Chang, Y.S. Hong, H.B. Chen, Thermochimica Acta, 397 (2003), 219-226.
7. L.M. Cafiero, G. Baffi, A. Chianese, R.J. Jachuck, Ind. Eng. Chem. Res., 41 (2002), 5240.
8. P. Hetherington, M.J. Scalley, R.J. Jachuck in: M. Cough,(Ed.) Fourth International Conference On Process Intensification For The Chemical Industry, Brugge, Belgium, 2001,145 - 153.
9. A.E. Nielsen, Acta Chem. Scand, 12 (1958), 951 - 958.
10. A.E. Nielsen, Acta Chem. Scand., 15 (1961), 441 - 442.
11. A.E. Nielsen, Kinetics of Precipitation, Pergamon, Oxford, 1964.
12. A.E. Nielsen, Krist. Technik, 4 (1969), 17 - 38.
13. R. Mohanty, A.I.Chem.E. J., 34 (1988), 2063.
14. C. Schwarzer, W. Peukert, A.I.Chem.E. J., 50 (2004), 3234.
15. C. Schwarzer, W. Peukert, Chem. Eng. Sci., 60 (2005), 11-25.
16. G. Trippa, R.J. Jachuck, Trans IChemE, 81 (2003), 766 - 772.
17. O. Sohnel, J. Garside, Precipitation: Basic Principles and Industrial Applications, Butterworth-Heinemann, Oxford, 1992.
18. P.W. Atkins, General Chemistry, Scientific American Books, 1989.
19. L.A. Bromley, A.I.Chem.E. J., 19 (1973), 313 - 320.
20. R.D. Cadle, Particle Size, Chapman-Hall, London, 1965.
21. A. Mersmann, Chemical Engineering and Processing, 38 (1999), 345-353.
22. A. Mersmann, B. Braun, M. Loffelmann, Chemical Engineering Science, 57 (2002), 4267-4275.
23. G.B. Tatterson, Scale-up And Design Of Industrial Mixing Processes, McGraw-Hill, New York, 1994.
24. J.N. Tilton, Fluid Particle Dynamics, in: R.H. Perry and D.W. Green, (Eds.), Perry's Chemical Engineering Handbook, McGraw-Hill, New York, 1998, p. 6-48.
25. R. Darby, Chem. Eng. Fluid Mech., Marcel Dekker, New York, 2001.

26. M. Roelands, et al., Chem. Eng. Technol., 26 (2003), 296.

27. P.A. Carosso, E. Pelizzetti, Journal of Crystal Growth, 68 (1984), 532-536.

28. J. Baldyga, J.R. Bourne, Turbulent Mixing And Chemical Reactions, Wiley, Chichester, 1999.

29. J. Villermaux, Micromixing Phenomena In Stirred Batch Reactors, Gulf Publishing, Houston, 1986.

30. J. Baldyga, J.R. Bourne, S.J. Hearn, Chemical Engineering Science, 52 (1997), 457-466.

31. A.A. Barresi, D. Marchisio, G. Baldi, Chemical Engineering Science, 54 (1999), 2339-2349.

32. J.S. Newman, Electrochemical Systems, 1st ed, Prentice-Hall, New Jersey, 1973.

33. S. Chakraborty, V. Balakotaiah, Chemical Engineering Science, 57 (2002), 2545-2564.

34. R.H. Perry, D.W. Green, J. Maloney, eds. Perry's Chemical Engineer's Handbook. McGraw-Hill: New York, 1998.

Table and Figure Captions

Table 1. Internal Dimensions of The Half-Channel (mm)

Table 2. Initial Supersaturations and Corresponding Mass Concentrations, m_i (g dm^{-3})

Table 3a. Calibration of Syringe Pump Driver For Narrow Channel Fluid Delivery for Channel A (Reactor I), d_h = 2.0 mm

Table 3b. Calibration of Syringe Pump Driver For Narrow Channel Fluid Delivery for Channel S2 (Reactor II), d_h = 0.5 mm

Table 4. Dilution Factors For $BaSO_4$ Suspension Samples In Diffraction Unit Circulation

Table 5. Time Scales and Characteristics Lengths of Turbulent Mixing [27] applicable to conditions used in this study (i.e. 61 < Re < 1025)

Figure 1. Schematic Plan-View of Channels A and B (Reactor I) With Mixing Junction, (Inset)

Figure 2. Schematic Plan-View of Channels S1 and S2 (Reactor II)

Figure 3. Cross-Section of One Half-Channel

Figure 4. Effect of (a) Channel Diameter And (b) Reynolds Number on Particle Sauter Diameter

Figure 5. (a) Comparison of PSDs for 0.5 mm Microchannel and Stirred Batch (b) Channel Reproducibility

Figure 6. Effects of (a) Channel Diameter And (b) Supersaturation on Particle Nucleation Rate

Figure 7. Effect of Reynolds Number on Particle Nucleation Rate

Figure 8. Effect of Reynolds Number on (a) Specific Power Input (b) Channel Pressure Drop

Figure 9. Effects of Peclet Number on (a) Sauter Diameter (b) Precipitate Conversion

Figure 10. Shear rate profile in narrow channels for 62 < Re < 1025

Figure 11. Effect of (a) Channel Diameter And (b) Supersaturation on Precipitate Conversion

Figure 12. SEM images for Channel S2 (d_h=0.5 mm) and S_0 = 2634 (a) (9 x 9)μm, (b) (1.2 x 1.2) μm

Figure 13. SEM images for (a) Channel S2 (d_h=0.5 mm) and S_0 = 4483, (9 x 9 μm), (b) Channel B (d_h=1.5 mm) S_0 = 4483 (9 x 9 μm)

TABLES

Table 1. Internal Dimensions of The Half-Channel (mm)

Channel	A	B	S1	S2
Side (d_h)	2.00	1.50	1.00	0.50
Depth	1.41	1.06	1.00	0.71
Width	2.82	2.12	2.00	1.42

Table 2. Initial Supersaturations and Corresponding Mass Concentrations, m_i (g dm^{-3})

Concentration	0.01M	0.02M	0.03M	0.04M	0.05M	0.075M	0.1M
$\mathbf{S_{act,0}}$	707	1265	1758	2211	2634	3602	4483
$\mathbf{m_{BaCl_2}}$	2.473	4.946	7.419	9.891	12.364	18.546	24.728
$\mathbf{m_{Na_2SO_4}}$	1.673	3.347	5.02	6.693	8.366	12.55	16.732

Table 3a. Calibration of Syringe Pump Driver for Narrow Channel Fluid Delivery for Channel A (Reactor I), d_h = 2.0 mm

Speed nom. % rate	Residence Time / [s]	Volumetric Flow [ml / s]	Mean Axial Vel. [m / s]	Reynolds Number
12.5	6.49	0.123	0.030	61.6
25.0	3.36	0.238	0.060	119.0
37.5	2.30	0.347	0.087	173.0
50.0	1.68	0.476	0.119	238.0
62.5	1.33	0.600	0.150	300.0
75.0	1.15	0.698	0.174	349.0
87.5	0.95	0.845	0.211	423.0
100.0	0.88	0.910	0.277	455.0

Table 3b. Calibration of Syringe Pump Driver For Narrow Channel Fluid Delivery for Channel S2 (Reactor II), d_h = 0.5 mm

Speed nom. % rate	Residence Time / [s]	Volumetric Flow [ml / s]	Mean Axial Vel. [m / s]	Reynolds Number
25.0	0.21	0.244	0.98	487
37.5	0.14	0.364	1.45	727
50.0	0.11	0.400	1.86	930
62.5	0.11	0.465	2.05	1025

Table 4. Dilution Factors For $BaSO_4$ Suspension Samples In Diffraction Unit Circulation

Initial Supersaturation, $S_{act,0}$	**Sample Volume, V_s / [ml]**	**Dilution Factor, $F = (V_s + 100) / V_s$**	**Error In Precipitate Yield / (%) For +/- 0.005 ml sample error**
707	3.0	34.3	0.16
2634	2.5	41.0	0.20
4483	1.5	67.6	0.35

Table 5. Time Scales and Characteristics Lengths of Turbulent Mixing [27] applicable to conditions used in this study (i.e. 61 < Re < 1025)

Time / Length-Scale	Expression	Units	62 <Re < 1025
Energy Dissipation, ε_{turb}	$\varepsilon_{turb} = \frac{Q\Delta P}{\rho V} = \frac{2fu^3}{d_h}$ $for_4f = 0.316\,Re^{-0.25}$ **(11)**	W kg^{-1}	0.001 – 482
Inertial-Convection, (τ_S)	$\tau_s = \frac{3}{4}\frac{L^{0.66}}{\varepsilon_{turb}^{0.33}}$ **(12)**	ms	82.0 – 1.00
Micro-mixing, (Kolmogorov), (τ_E)	$\tau_E = \frac{1}{E} = 17.24\left(\frac{\nu}{\varepsilon_{turb}}\right)^{0.5}$ **(13)**	ms	545.0 – 0.78
Molecular Diffusion, (Batchelor) (τ_{diff})	$\tau_{diff} = \frac{\eta^2{}_B}{D_m}$ **(14)**	ms	25.0 – 0.03
Kolmogorov Length Scale	$\eta_k = \left(\frac{\nu^3}{\varepsilon_{turb}}\right)^{0.25}$ **(15)**	μm	187.0 – 6.00
Batchelor Length Scale	$\eta_B = \eta_k Sc^{-0.5}$ **(16)**	μm	1.87 – 0.06

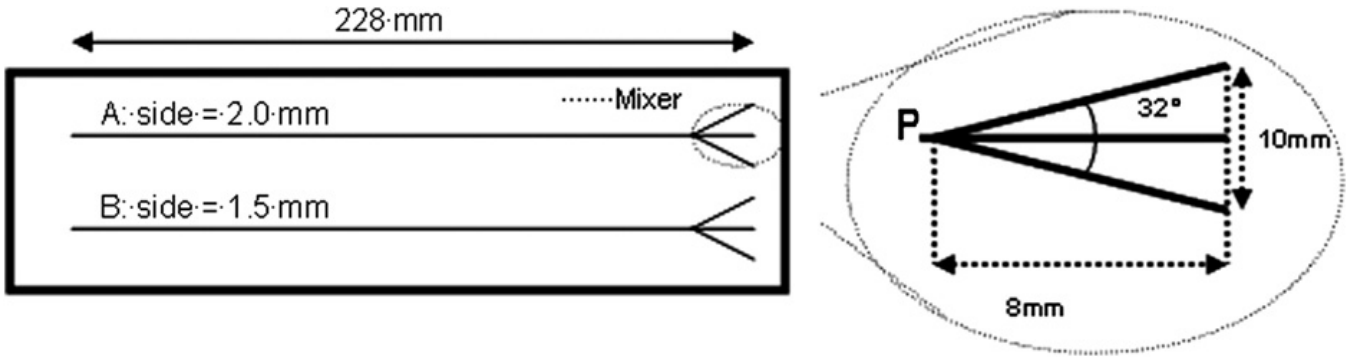

Figure 1. Schematic Plan-View of Channels A and B (Reactor I) With Mixing Junction, (Inset)

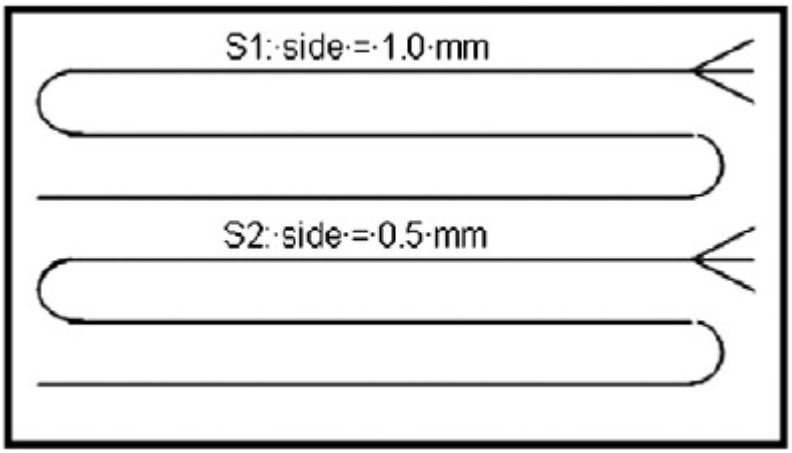

Figure 2. Schematic Plan-View of Channels S1 and S2 (Reactor II)

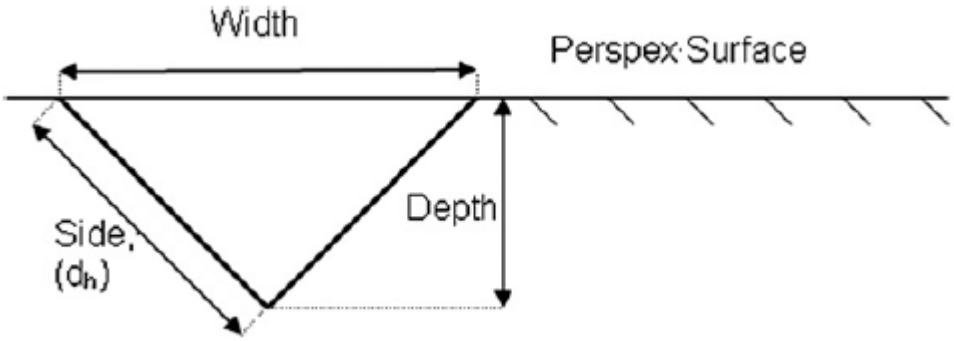

Figure 3. Cross-Section of One Half-Channel

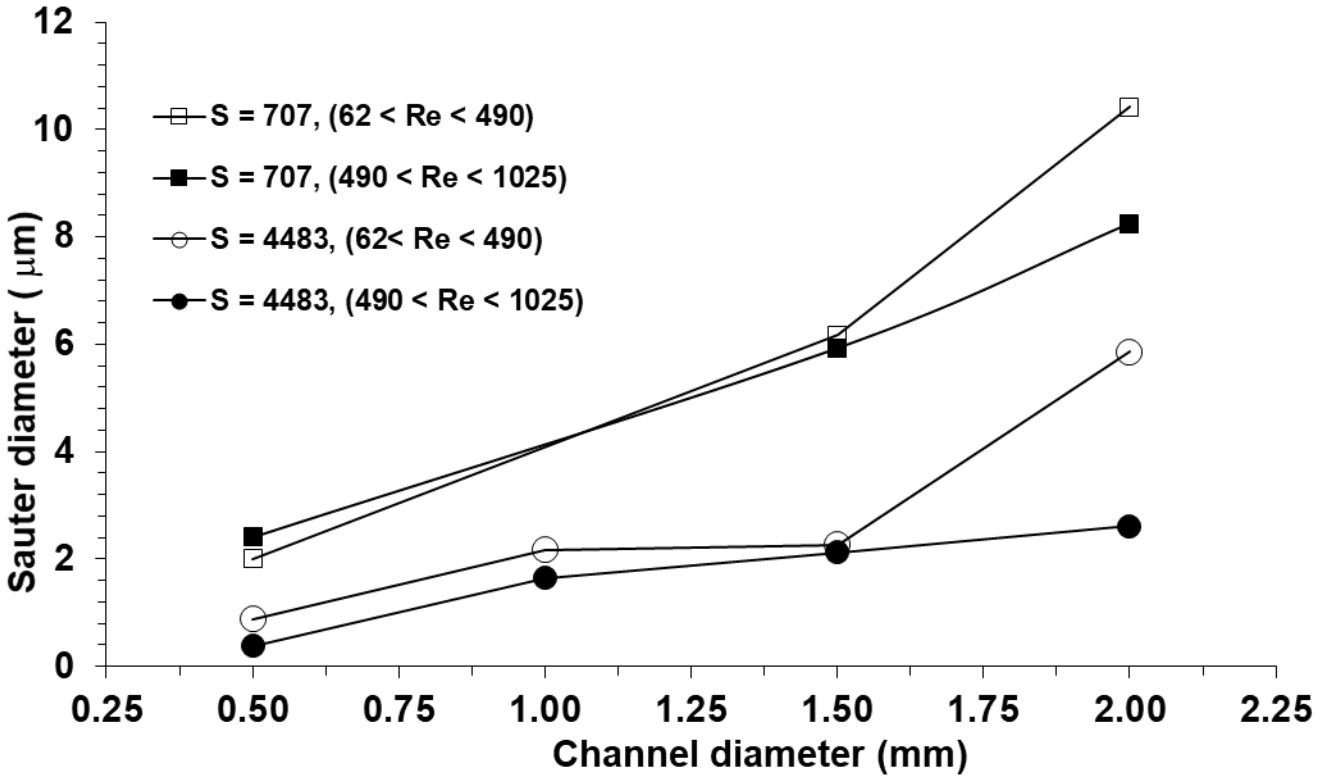
S = 707, (62 < Re < 490)
S = 707, (490 < Re < 1025)
S = 4483, (62< Re < 490)
S = 4483, (490 < Re < 1025)
Sauter diameter (μm)
Channel diameter (mm)
0
2
4
6
8
10
12
0.25
0.50
0.75
1.00
1.25
1.50
1.75
2.00
2.25

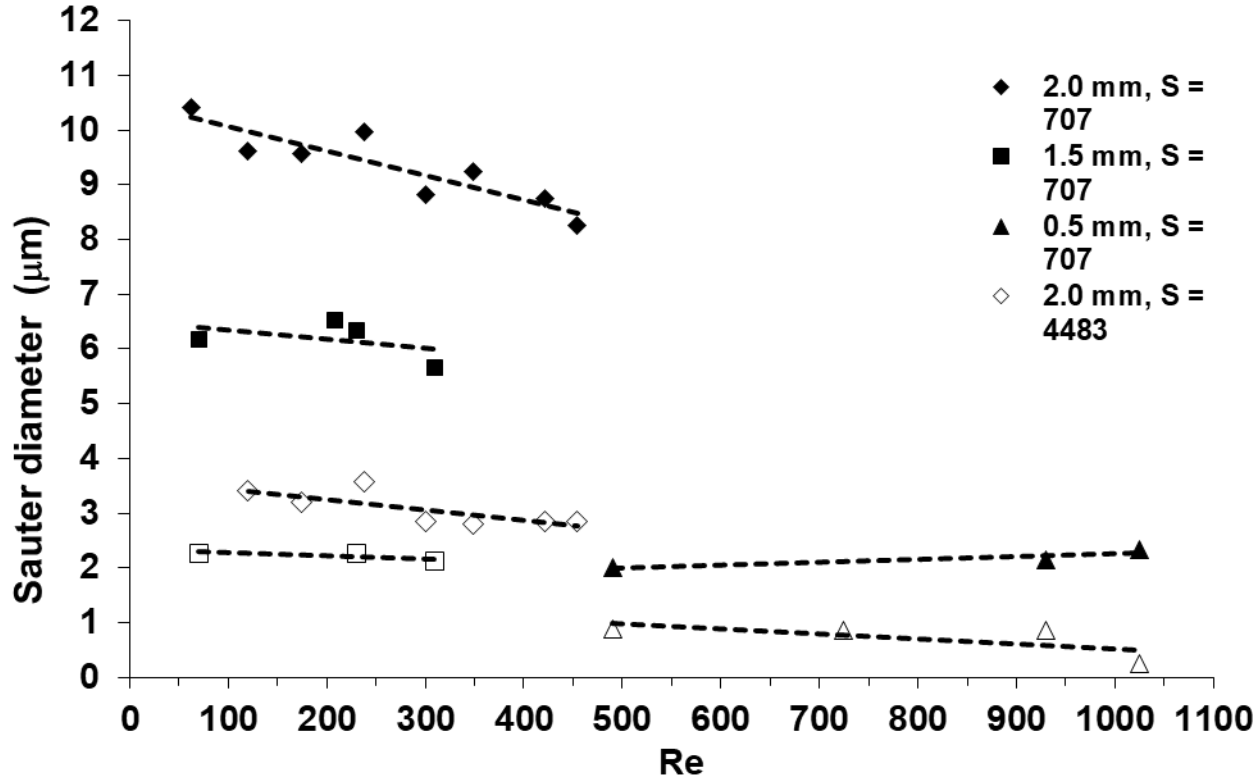
2.0 mm, S = 707
1.5 mm, S = 707
0.5 mm, S = 707
2.0 mm, S = 4483
Sauter diameter (μm)
Re
0
1
2
3
4
5
6
7
8
9
10
11
12
0
100
200
300
400
500
600
700
800
900
1000
1100

Figure 4. Effect of (a) Channel Diameter And (b) Reynolds Number on Particle Sauter Diameter

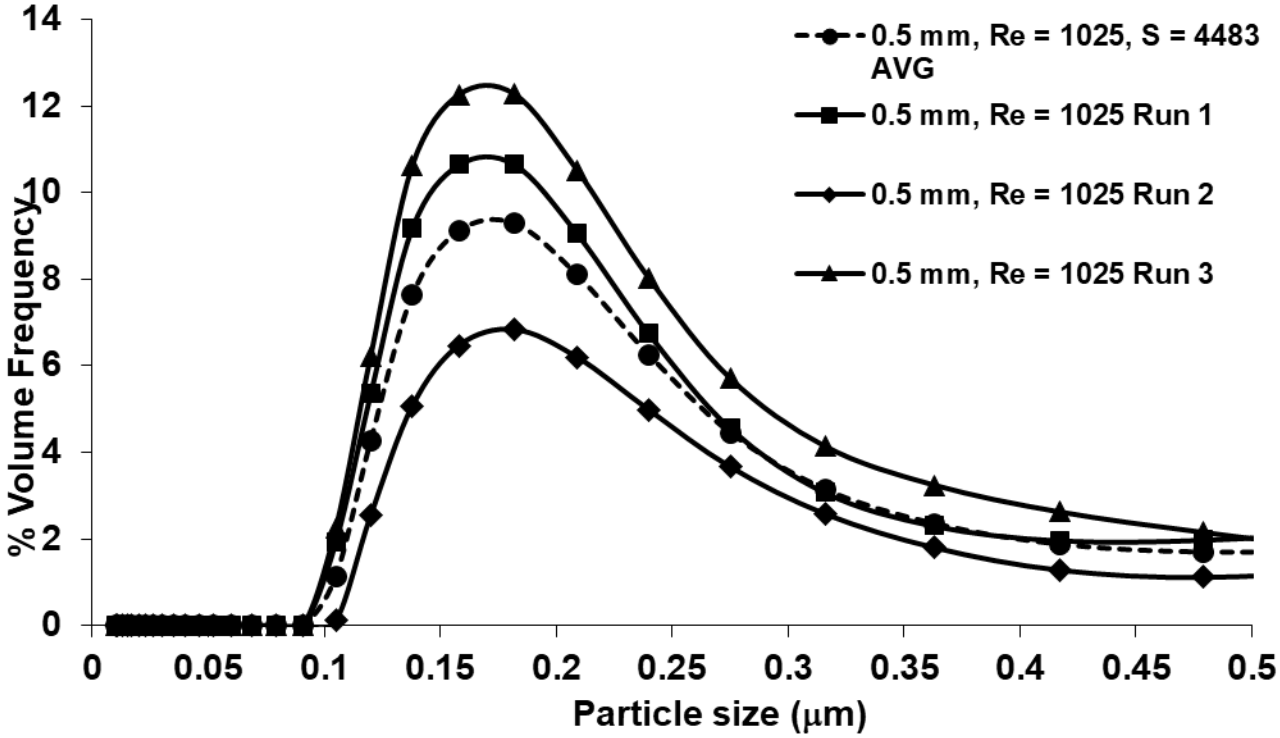

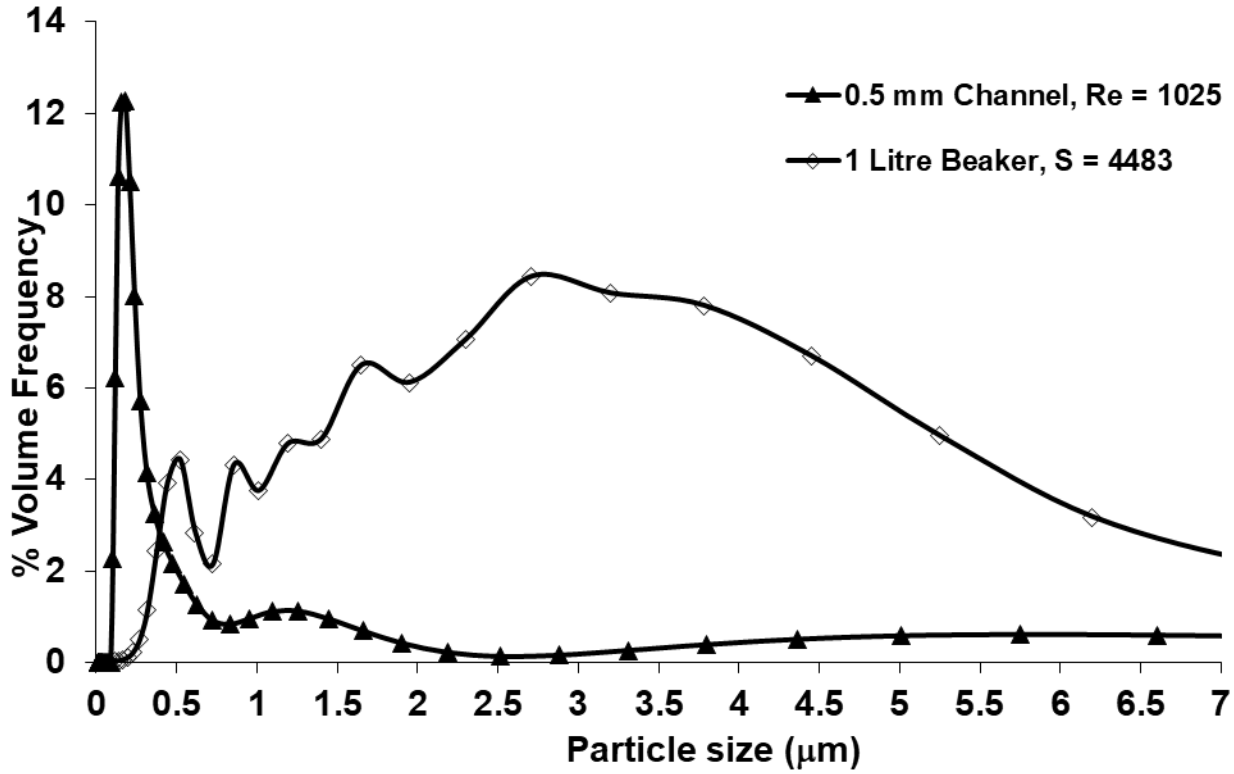

Figure 5. (a) Comparison of PSDs for 0.5 mm Microchannel and Stirred Batch (b) Channel Reproducibility

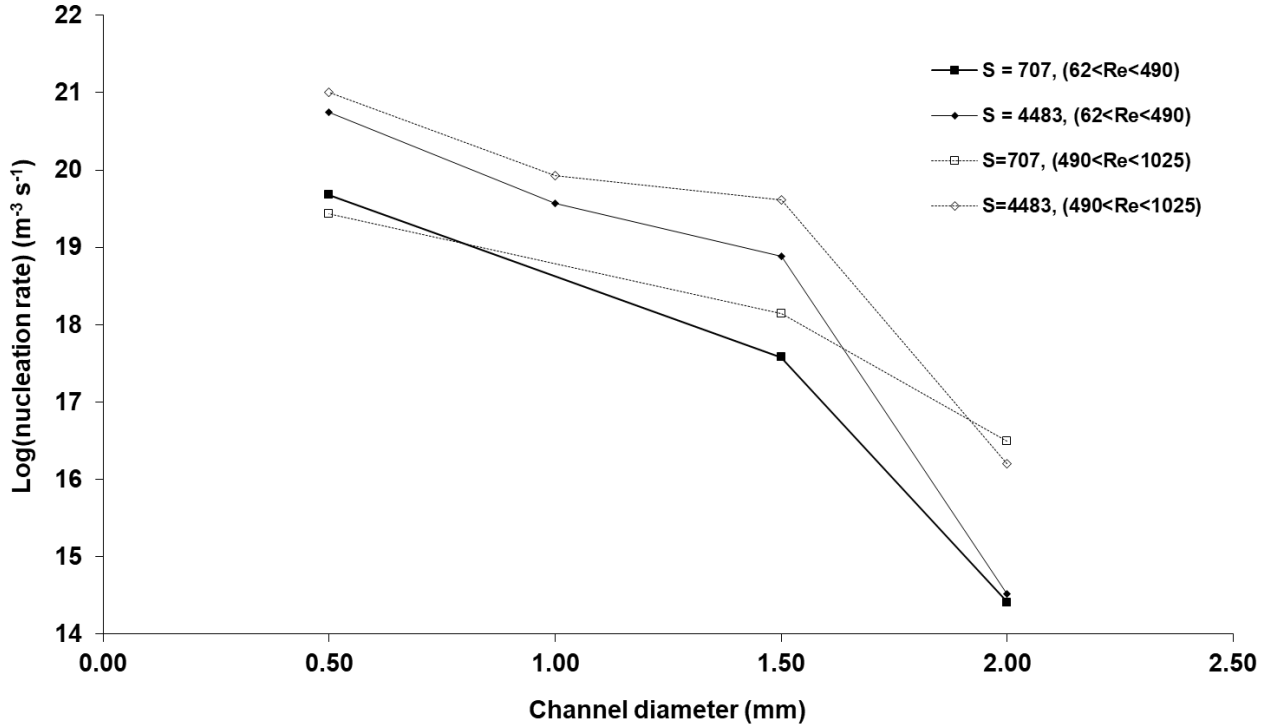
Log(nucleation rate) (m-3 s-1)
Channel diameter (mm)
S = 707, (62<Re<490)
S = 4483, (62<Re<490)
S=707, (490<Re<1025)
S=4483, (490<Re<1025)

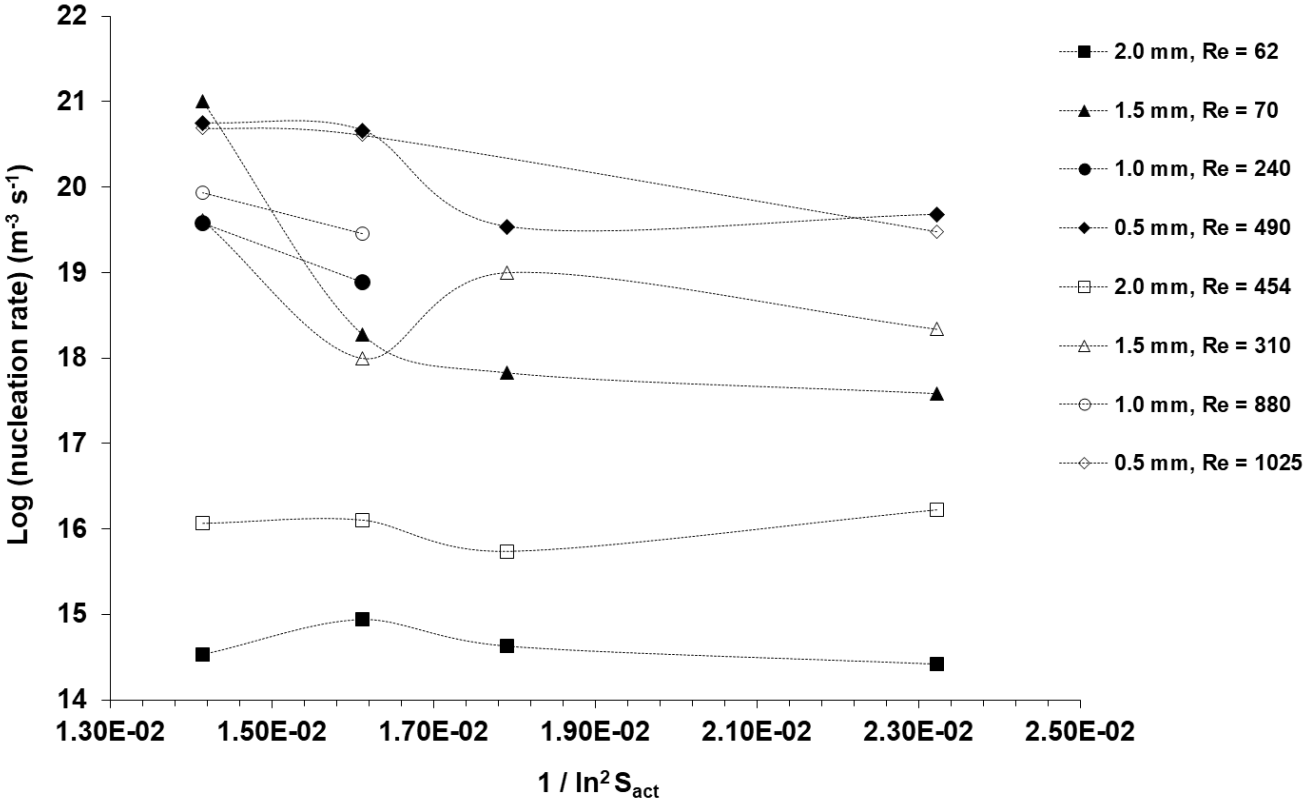
Log (nucleation rate) (m-3 s-1)
1 / ln2 Sact
2.0 mm, Re = 62
1.5 mm, Re = 70
1.0 mm, Re = 240
0.5 mm, Re = 490
2.0 mm, Re = 454
1.5 mm, Re = 310
1.0 mm, Re = 880
0.5 mm, Re = 1025

Figure 6. Effects of (a) Channel Diameter And (b) Supersaturation on Particle Nucleation Rate

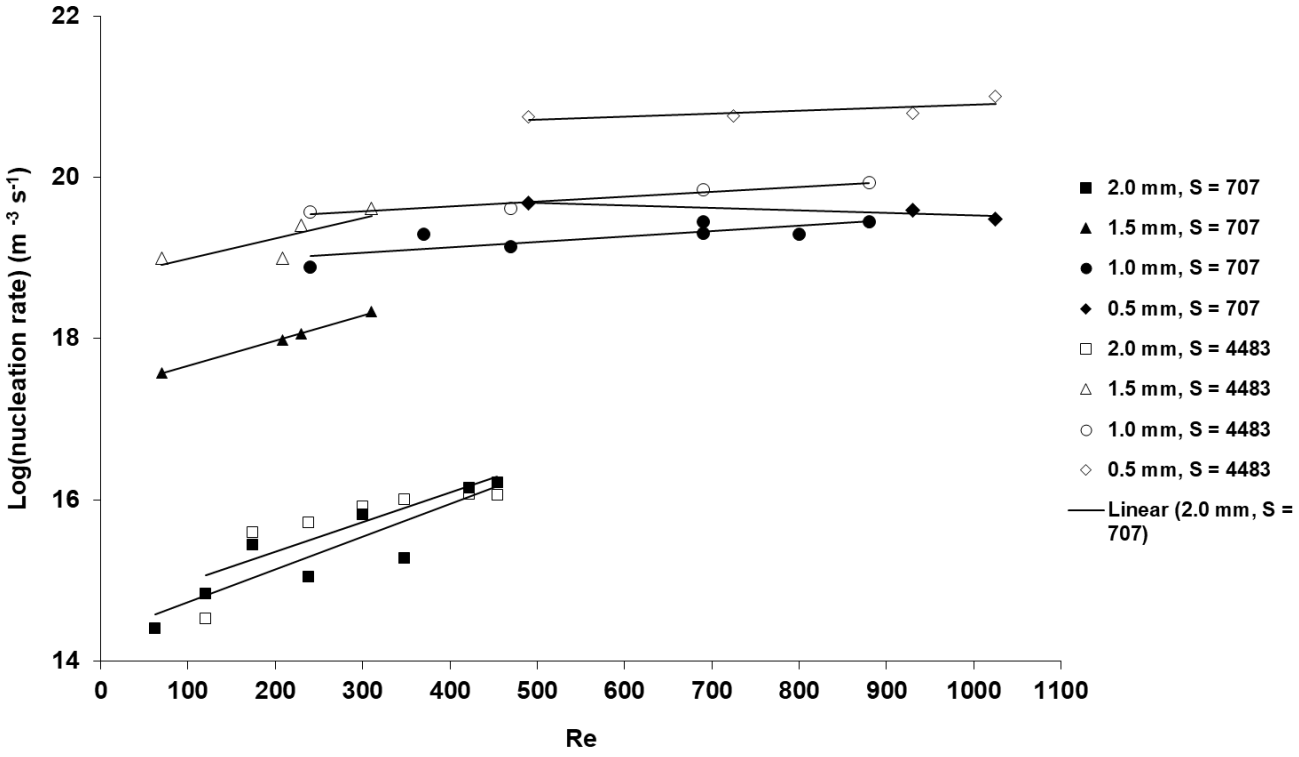

Figure 7. Effect of Reynolds Number on Particle Nucleation Rate

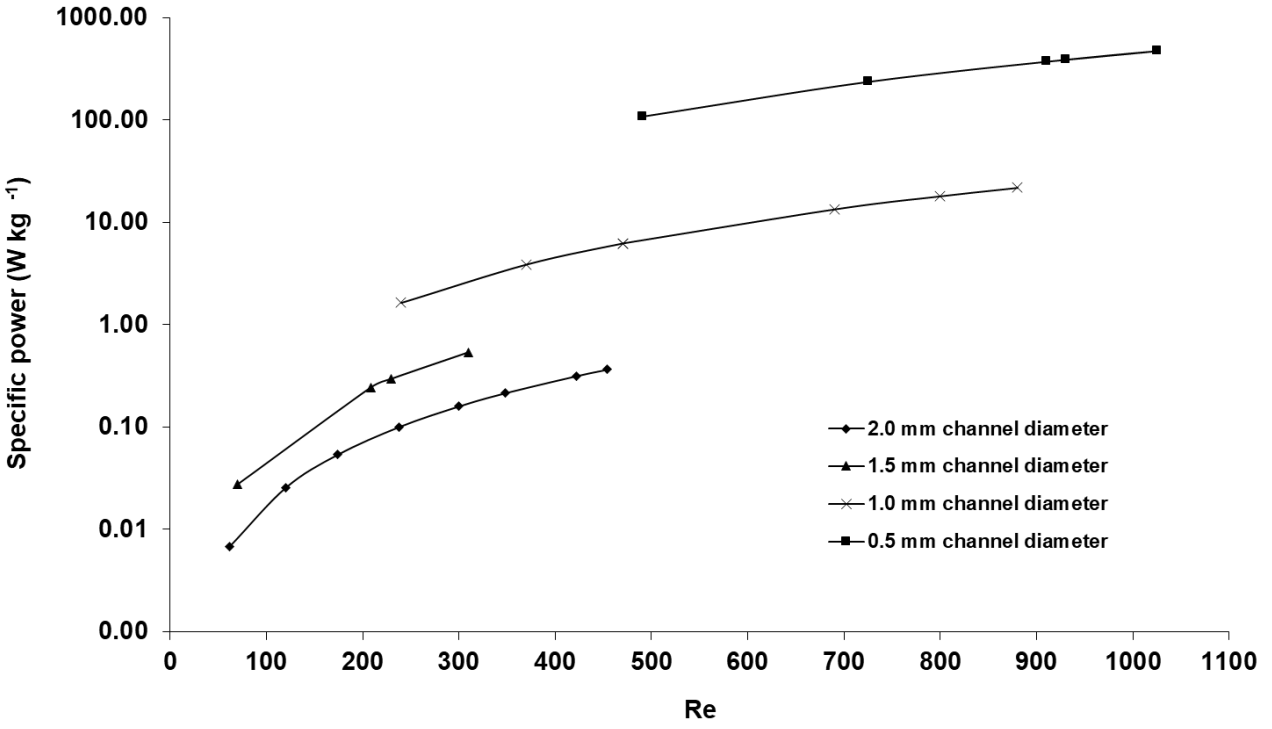

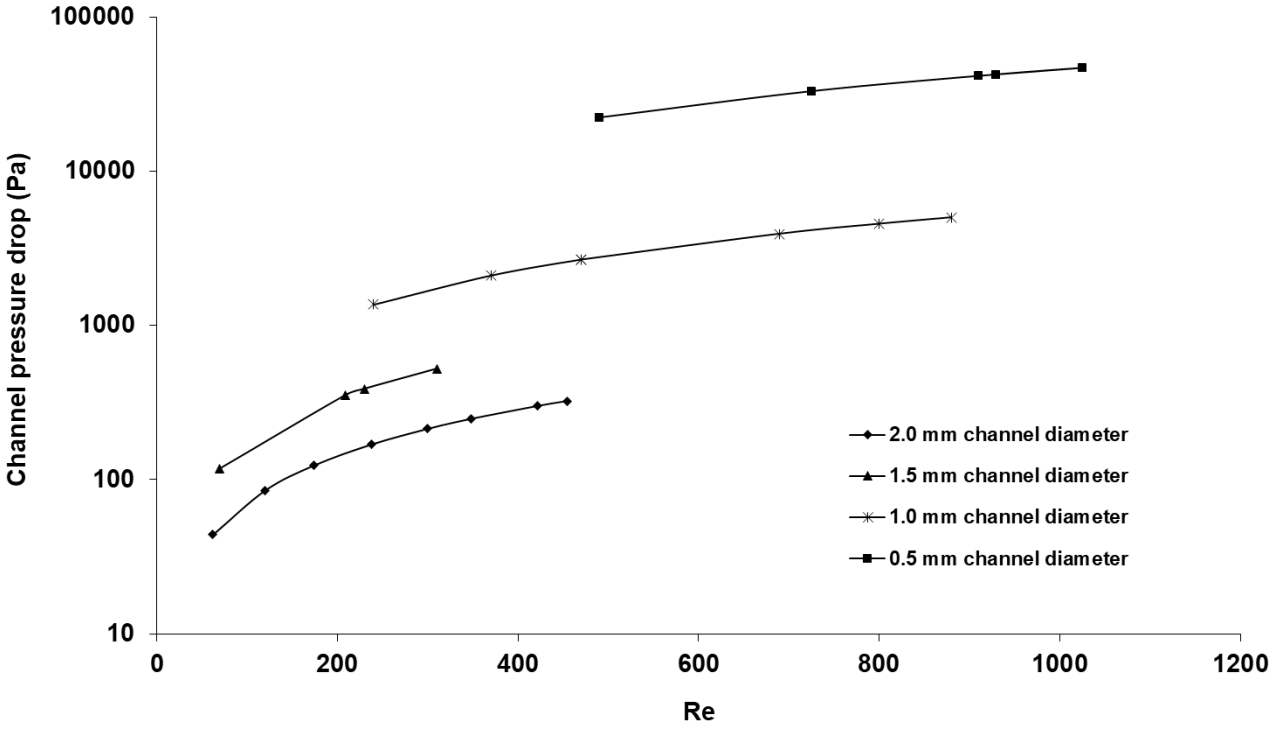

Figure 8. Effect of Reynolds Number on (a) Specific Power Input (b) Channel Pressure Drop

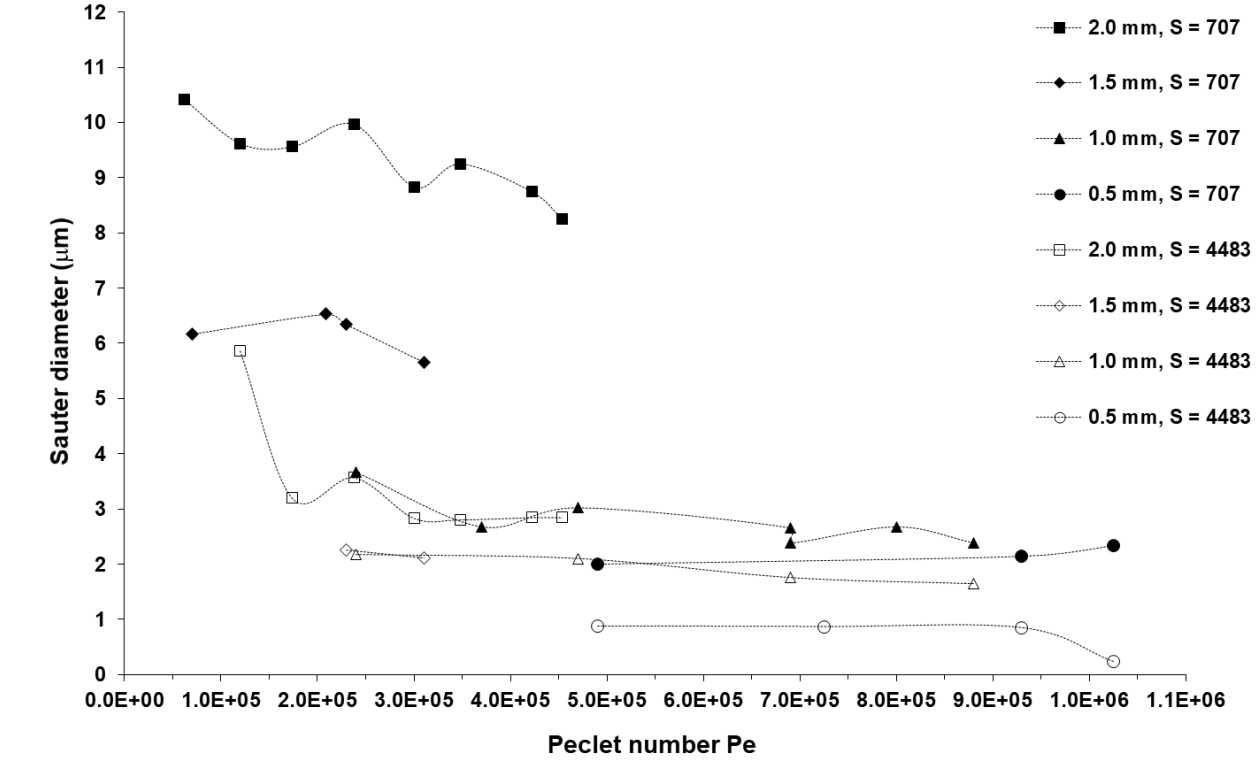

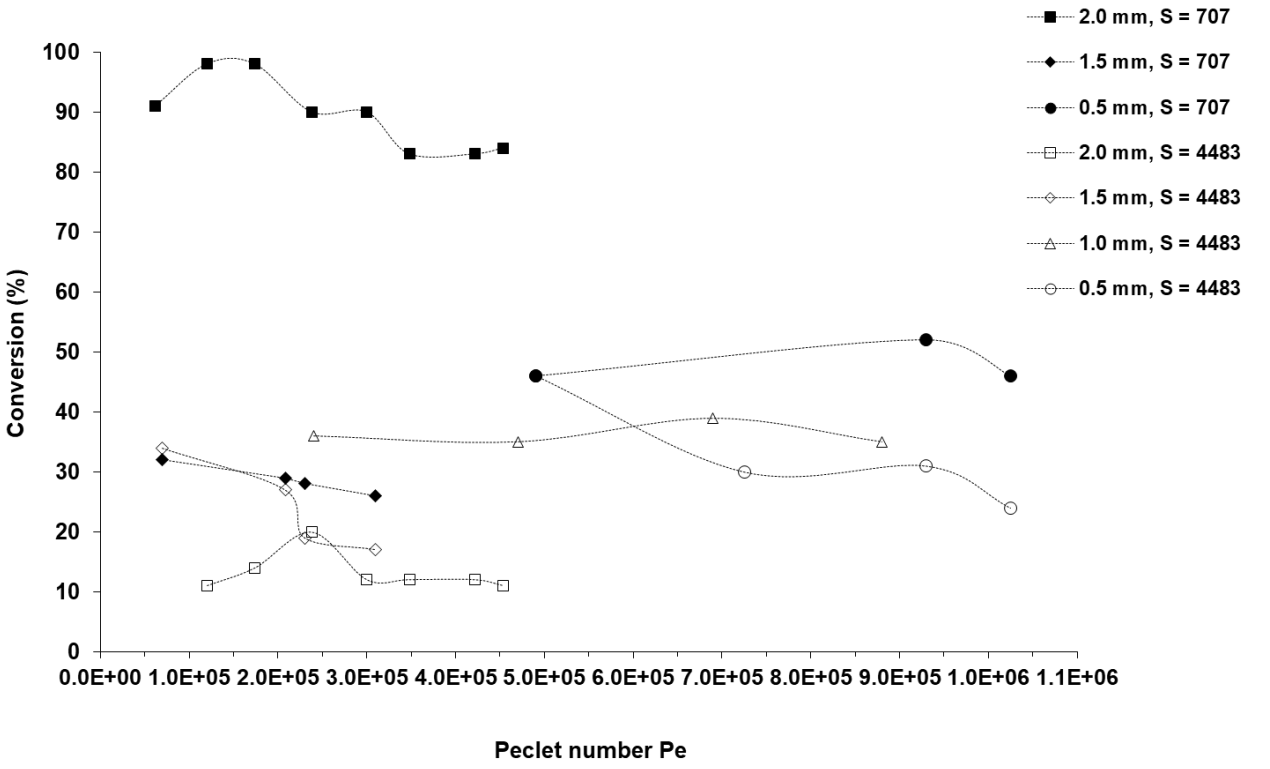

Figure 9. Effects of Peclet Number on (a) Sauter Diameter (b) Precipitate Conversion

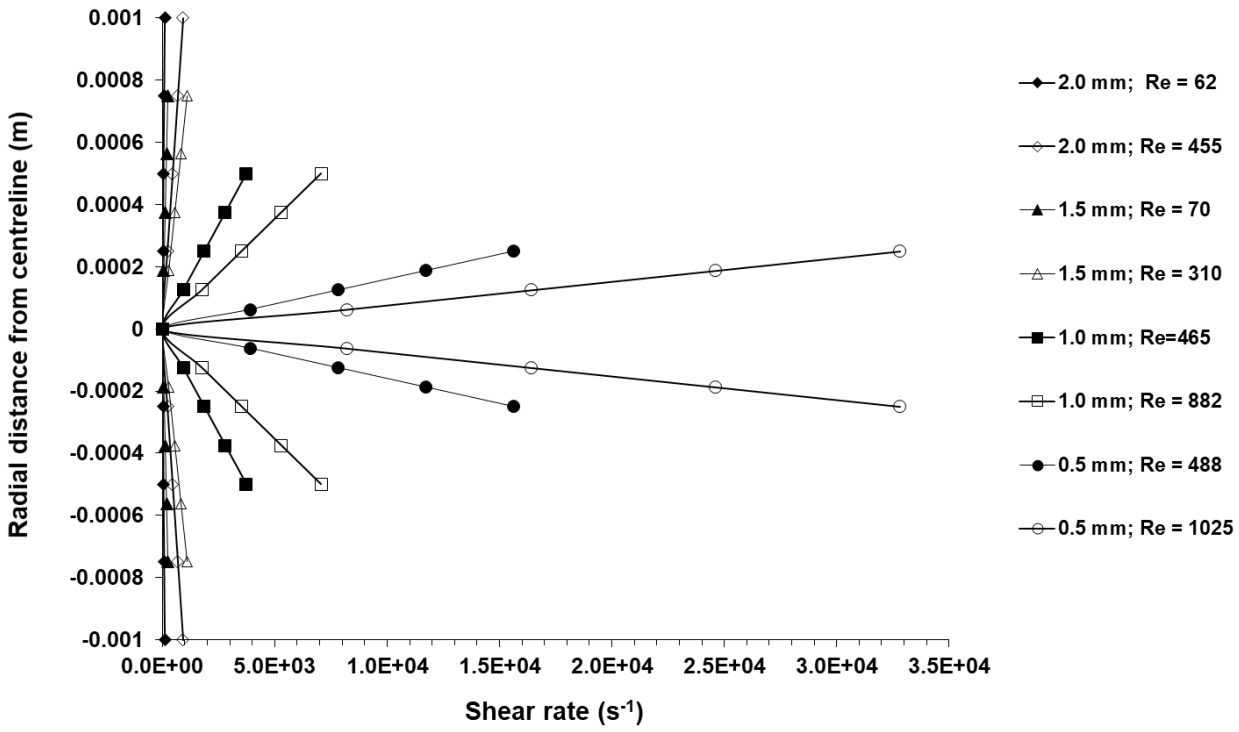

Figure 10. Shear rate profile in narrow channels for 62 < Re < 1025

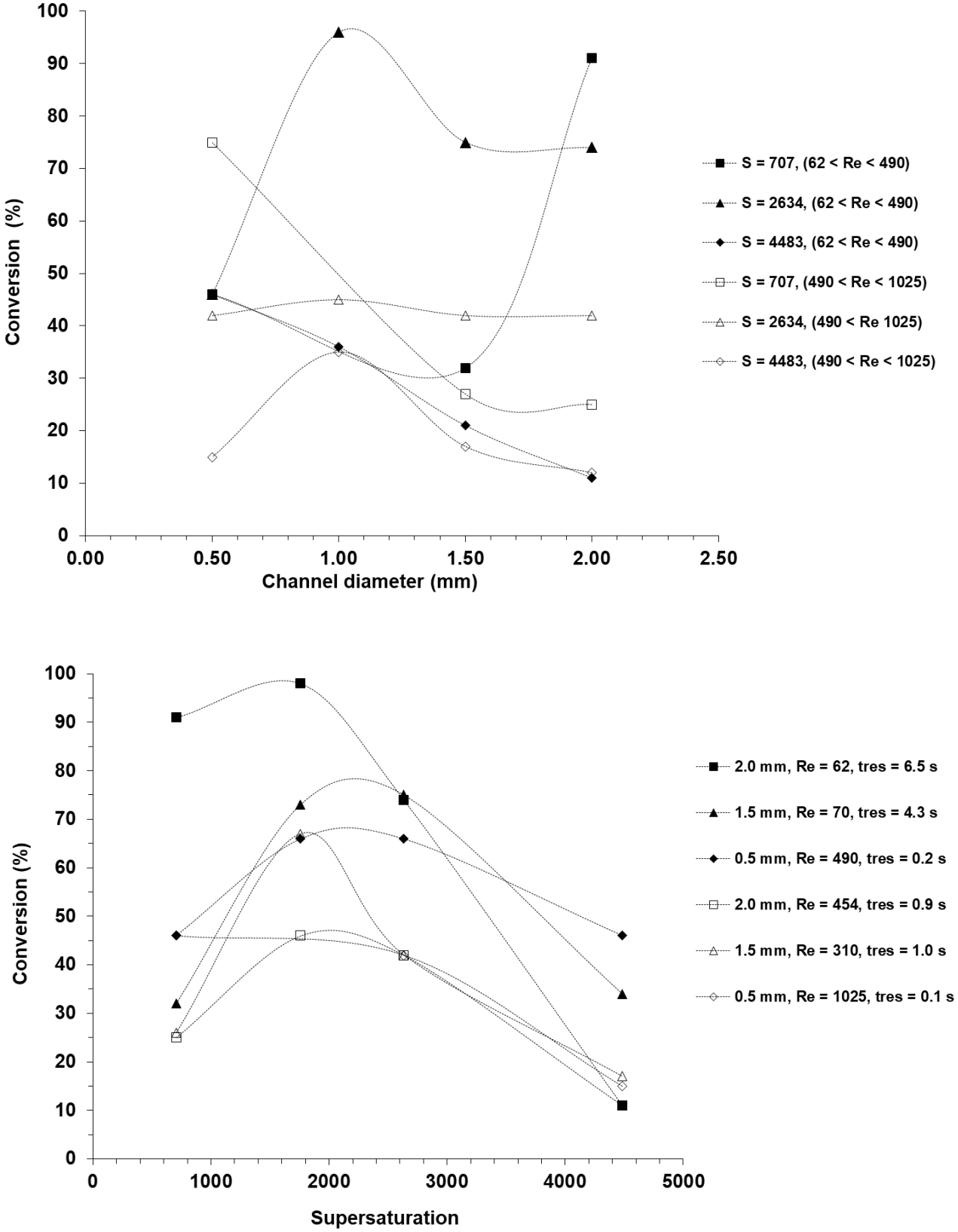

Figure 11. Effect of (a) Channel Diameter And (b) Supersaturation on Precipitate Conversion

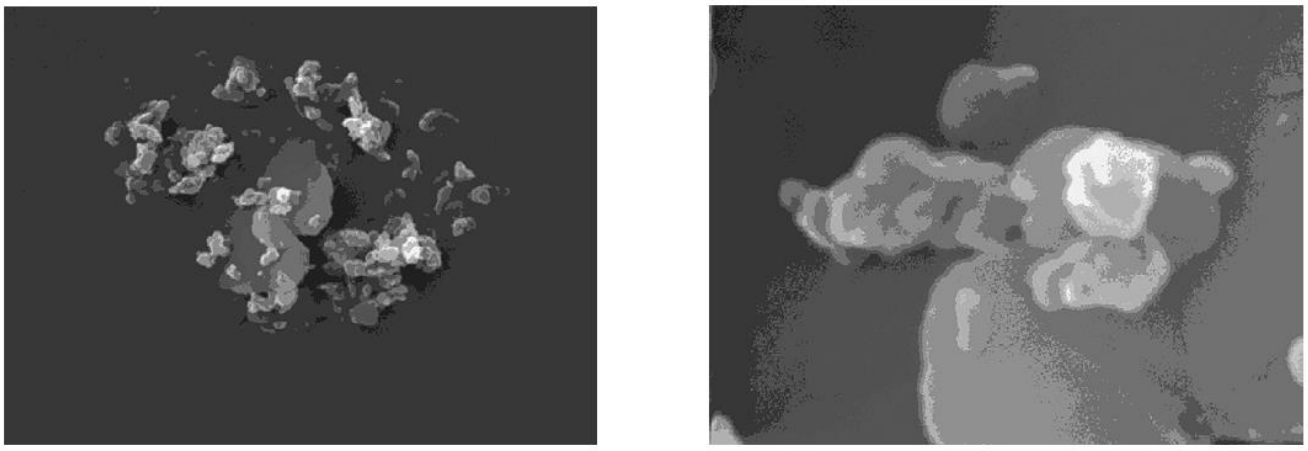

(a) (b)

Figure 12. SEM images for Channel S2 (d_h=0.5 mm) and S_0 = 2634 (a) (9 x 9)μm, (b) (1.2 x 1.2) μm

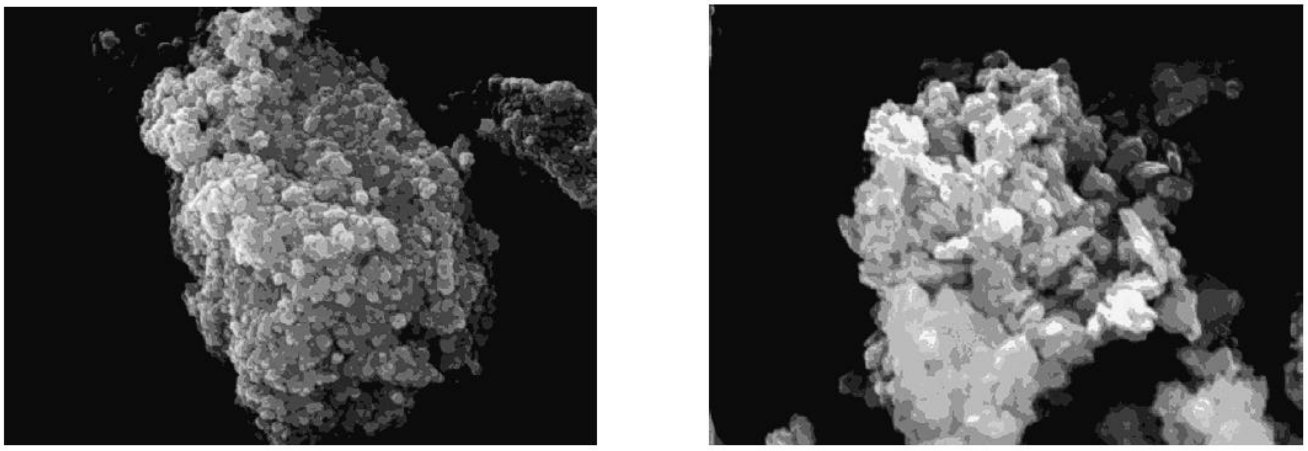

(a) (b)

Figure 13. SEM images for (a) Channel S2 (d_h=0.5 mm) and S_0 = 4483, (9 x 9 μm), (b) Channel B (d_h=1.5 mm) S_0 = 4483 (9 x 9 μm)